Syndapin and GTPase RAP-1 Control Endocytic Recycling via RHO-1 and Non-Muscle Myosin II

Wilmer R. Rodriguez-Polanco[1], Anne Norris[1], Agustin B. Velasco[1], Adenrele M. Gleason[1], and Barth D. Grant[1, 2]*

[1]Department of Molecular Biology and Biochemistry Rutgers University, Piscataway, New Jersey 08854, United States of America.

[2]Rutgers Center for Lipid Research

* barthgra@dls.rutgers.edu

Abstract

After endocytosis, many plasma membrane components are recycled via narrow-diameter membrane tubules that emerge from early endosomes to form recycling endosomes, eventually leading to their return to the plasma membrane. We previously showed that the F-BAR and SH3 domain Syndapin/PACSIN-family protein SDPN-1 is required *in vivo* for basolateral endocytic recycling in the *C. elegans* intestine. Here we sought to determine the significance of a predicted interaction between the SDPN-1 SH3 domain and a target sequence in PXF-1/PDZ-GEF1/RAPGEF2, a known exchange factor for Rap-GTPases. We found that endogenous mutations we engineered into the SDPN-1 SH3 domain, or its binding site in the PXF-1 protein, interfere with recycling *in vivo*, as does loss of the PXF-1 target RAP-1. Rap-GTPases have been shown in several contexts to negatively regulate RhoA activity. Our results show that RHO-1/RhoA is enriched on SDPN-1 and RAP-1 positive endosomes in the *C. elegans* intestine, and loss of SDPN-1 or RAP-1 elevates RHO-1(GTP) levels on intestinal endosomes. Furthermore, we found that depletion of RHO-1 suppressed *sdpn-1* mutant recycling defects, indicating that control of RHO-1 activity is a key mechanism by which SDPN-1 acts to promote endocytic recycling. RHO-1/RhoA is well-known for controlling actomyosin contraction cycles, although little is known of non-muscle myosin II on endosomes. Our analysis found that non-muscle myosin II is enriched on SDPN-1 positive endosomes, with two non-muscle myosin II heavy chain isoforms acting in apparent opposition. Depletion of *nmy-2* inhibited recycling like *sdpn-1* mutants, while depletion of *nmy-1* suppressed *sdpn-1* mutant recycling defects, indicating actomyosin contractility in controlling recycling endosome function.

22 # Introduction

23 Cells internalize extracellular material, receptor-associated ligands, membrane proteins and
24 lipids by endocytosis (1). Uptake mechanisms can be generally divided into clathrin-dependent
25 and clathrin-independent endocytosis (CDE and CIE, respectively), after which internalized
26 cargo is sorted within endosomes for delivery to distinct intracellular destinations (2). As
27 membrane and fluid are added to the early endosome by incoming vesicles, narrow-diameter
28 recycling tubules form, collecting a subset of cargo (3). Most plasma membrane lipids, and
29 many types of internalized transmembrane proteins, are recycled back to the plasma
30 membrane either directly (rapid recycling), indirectly via the endocytic recycling compartment
31 (ERC) (slow recycling), or Golgi (retrograde recycling) (3, 4). As early endosomes mature they
32 become late endosomes, eventually fusing with lysosomes, promoting degradation of
33 remaining cargo. Many cellular processes depend upon accurate and efficient endocytic
34 recycling, including cell migration, cell division, cell-cell fusion events, and control of neuronal
35 signaling during learning and memory (3, 4). Trafficking pathways are often more elaborate in
36 the context of polarized cells such as epithelia and neurons that maintain multiple functionally
37 distinct plasma membrane domains, e.g. basolateral versus apical in epithelia, and dendrite
38 versus axon in neurons (4).

39 The *C. elegans* intestine is a polarized epithelial tube consisting of exactly 20 cells that form
40 nine donut-like rings, the most anterior ring consisting of four symmetrical cells and all other
41 rings comprised of two cells (5, 6). The intestinal cells have a basolateral surface that faces the
42 pseudocoelom and controls the exchange of molecules between the intestine and the rest of

43 the body (5). The microvilli-rich apical surface faces the central lumen and is important for
44 nutrient uptake (6). We previously developed the *C. elegans* intestine as a model system for the
45 study of polarized epithelial trafficking mechanisms, allowing analysis of transport in the native
46 context of a polarized-epithelial tube within the intact living animal (7-10). Taking advantage of
47 the *C. elegans* intestinal system, our laboratory previously showed that *C. elegans* SDPN-1, a
48 Syndapin/PACSIN family protein, is important for basolateral endocytic recycling *in vivo,* a
49 finding confirmed independently by others (9, 11).

50 Syndapin/PACSIN family proteins bear a single N-terminal F-BAR domain and a single C-terminal
51 SH3 domain. BAR domains in general, including the F-BAR subclass, are known to sense
52 membrane curvature and to promote positive curvature, properties likely to help drive
53 membrane budding and tubulation (12). Our previous work showed that *C. elegans* SDPN-1 is
54 essential for the basolateral recycling of cargo proteins that are transported via the early
55 endosome–to–recycling endosome route, but not other routes (Gleason et al., 2016). Affected
56 cargos accumulate at much higher-than-normal levels in the endosomes of *sdpn-1* mutants
57 (Gleason et al., 2016). These include well characterized model cargo proteins hTAC (human IL-2
58 receptor α-chain), hTFR (human transferrin receptor), and DAF-4 (type-II TGF-β receptor), but
59 not MIG-14/Wls or SMA-6 (type-I TGF-β receptor) that recycle via the retromer pathway, or
60 CD4-LL that does not recycle (Gleason et al., 2016). SDPN-1 protein is highly enriched on early
61 and basolateral recycling endosomes of the intestinal cells, and *sdpn-1 null* mutants display
62 abnormal accumulation of early and basolateral recycling endosomes, suggesting a direct role
63 in their regulation (Gleason et al. 2016). Mammalian Syndapin2 is also well known to associate
64 with recycling endosome proteins and to promote endocytic recycling, but many questions

65 remain about the mechanism by which Syndapin/PACSIN proteins regulate endosomal function
66 (13-15).

67 To better understand how SDPN-1 promotes recycling we sought to identify partner proteins
68 relevant to recycling, with a particular focus on results from the *C. elegans* SH3-ome project
69 (16). Here we investigated one high-confidence hit for the SDPN-1 SH3 domain, PXF-1/PDZ-GEF,
70 an exchange factor for the small Ras-like GTPase RAP-1/Rap (17, 18). Importantly we show that
71 PXF-1 and its target RAP-1 also regulate recycling like SDPN-1, and interfering with the
72 interaction of SDPN-1 and PXF-1 disrupts recycling. We trace the activity of RAP-1 on
73 endosomes to negative regulation of RHO-1 and myosin II heavy chain isoform NMY-1, and
74 show that reduction in RHO-1 or NMY-1 greatly ameliorates *sdpn-1* mutant trafficking defects.
75 This function appears to work in opposition to myosin II heavy chain isoform NMY-2 that we
76 find is required for recycling. Taken together our results indicate that myosin II regulation is a
77 key output of endosomal SDPN-1 that is essential to maintain recycling function.

78

79 # Materials and Methods

80 **General methods and strains**

81 All *C. elegans* strains were derived from Bristol strain N2 and cultured at 20°C on NGM plates
82 seeded with the *Escherichia coli* strain OP50. A list of strains used in this study can be found in
83 Supplemental Table 1.

84 **Transgenic Strains**

85 To construct GFP or RFP fusion transgenes for expression in the worm intestine, Gateway
86 destination vectors were used. Each vector contained the promoter region of the intestine-
87 specific gene *vha-6*, followed by GFP, mScarlet, or tagRFP coding sequences, a Gateway
88 cassette (Invitrogen, Carlsbad, CA), and *let-858* 3' UTR sequences. The genomic or cDNA
89 sequences of *C. elegans* genes were cloned individually into entry vector pDONR221. Mutant
90 forms of the coding regions were obtained using site-directed mutagenesis using the
91 Quikchange II kit (Stratagene). Coding regions were transferred into P*vha-6*-GFP or P*vha-6*-RFP
92 vectors by LR reaction (Invitrogen). Constructs were bombarded into *unc-119(ed3)* mutant
93 animals to establish low copy integrated transgenic lines, or integrated in single copy using the
94 MiniMos system and Hygromycin or G418 selection (19).

95 **RNAi**

96 *C. elegans* RNAi-mediated interference was performed as described (20). Feeding constructs in
97 this study were from the Ahringer library, except for *rho-1*, for which a cDNA was cloned into
98 the L4440/pPD129.36 vector between unique SacI and HindIII sites (21). RNAi clones for *nmy-1*
99 and *nmy-2* were kindly provided by Adriana Dawes (Ohio State University) (22). For most RNAi
100 experiments, synchronized L4 stage animals were grown on RNAi plates at 20°C. After the first
101 generation, we transferred about 60 L4 stage animals to fresh RNAi plates at 20°C for another
102 24 hours prior to imaging as young adults.

103 **Protein Expression, Pulldown Assays, and Western Analysis**

104 N-terminally hemagglutinin (HA)-tagged PXF-1 protein, amino acids 1-477, with or without
105 mutation of the predicted SDPN-1 binding site, was synthesized *in vitro* using the TNT-coupled
106 transcription-translation system (Promega, Madison, WI) using DNA templates pcDNA3.1–
107 2xHA-PXF-1 and pcDNA3.1–2xHA-PXF-1(K191/P195/P198->AAA), respectively (1.6 ug/each 50-
108 ul reaction). The reaction cocktail was incubated at 30°C for 90 min. Control glutathione *S*-
109 transferase (pGEX-2T), GST-SDPN-1 SH3 (final 112 amino acids), and GST-SDPN-1 SH3 (P479L)
110 fusion proteins were expressed in the *ArcticExpress* strain of *Escherichia coli* (Stratagene, La
111 Jolla, CA). Bacterial pellets were lysed in 10 ml B-PER Bacterial Protein Extraction Reagent
112 (Pierce, Rockford, ILL) with Complete Protease Inhibitor Cocktail Tablets (Roche, Indianapolis,
113 IN). Extracts were cleared by centrifugation, and supernatants were incubated with
114 glutathione-Sepharose 4B beads (Amersham Pharmacia, Piscataway, NJ) at 4°C overnight.
115 Beads were then washed six times with cold STET buffer (10 mM Tris-HCl, pH 8.0, 150 mM NaCl,
116 1 mM EDTA, 0.1% Tween-20). In vitro–synthesized HA-tagged protein (10 ul TNT mix diluted in
117 500 ul STET) was added to the beads and allowed to bind at 4°C for 2 h. After six additional
118 washes in STET the proteins were eluted by boiling in 30 ul 2X-SDS-PAGE sample buffer. Eluted
119 proteins were separated on SDS-PAGE, blotted to nitrocellulose, visualized with Ponceau S and
120 scanned, then washed to remove Ponceau staining, and probed with anti-HA (16B12)
121 antibodies and HA-conjugated secondary antibodies (Pierce). Detection was achieved using
122 Super Signal West Pico detection system (Pierce).

123 **CRISPR**

124 *sdpn-1* P479L and *pxf-1* K191/P195/P198->AAA mutations were introduced into the
125 endogenous genes in *C. elegans* using the *dpy-10* co-CRISPR technique as described by Paix and
126 Seydoux (23), creating mutant alleles *sdpn-1(pw33)* and *pxf-1(pw34)*. 3XFLAG-GFP was inserted
127 into the *pxf-1* gene between the last codon and stop codon using the SEC selection technique
128 described by Dickinson as modified by Schwartz (24, 25).

129 **Microscopy and image analysis**

130 Imaging was performed on live first-day adult hermaphrodites animals mounted on slides using
131 5% agarose pads with 10 mM levamisole. Most single channel data in Figure 2 was captured on
132 a Zeiss LSM 710 confocal microscope. All other single channel data, including Figure **2B**-**B',** was
133 captured on a Zeiss LSM 800 confocal microscope. For both microscopes, the LSM 710 and LSM
134 800, GFP tagged protein image acquisition used the 488 nm laser line and the 63X (1.4 NA)
135 objective and ZEISS ZEN 2.3 imaging software. True GFP signal was separated from the broad-
136 spectrum auto-fluorescence displayed by the lysosome-related organelles (gut granules) of the
137 *C. elegans* intestine using the Spectral Fingerprinting and Linear Unmixing functions in ZEN. The
138 images were exported as TIF files for analysis in Metamorph version 7.7 software.

139 The "Integrated Morphometry Analysis" function of Metamorph was used to measure
140 fluorescence intensity, puncta number (structure count), and fluorescence area (total area)
141 within unit regions. At least 9 animals were used for each analysis. Fluorescence signal in the
142 basolateral membrane between two neighboring cells was avoided for the analysis.

143 For multiwavelength fluorescence colocalization studies, images were obtained using a
144 spinning-disk confocal imaging system: Axiovert Z1 microscope (Carl Zeiss Microimaging)
145 equipped with a X-Light V2 Spinning Disk Confocal Unit (CrestOptics), 7-line LDI Laser Launch
146 (89 North), Prime 95B Scientific CMOS camera (Photometrics) and 63X and 100X oil-immersion
147 objectives. Data were captured as an image stack with 0.2 µm step size using Metamorph
148 version 7.7 software (Universal Imaging), and deconvolved using Autoquant X3 (Media
149 Cybernetics). In Metamorph, a single plane from each image stack (either top plane or middle
150 plane) was chosen in which both markers were clearly visible. In the middle plane of the worm
151 intestine, the apical membranes and the basolateral membranes are visible, while on top plane
152 images only the basolateral membrane is visible. Images taken in the DAPI channel were used
153 to identify broad-spectrum intestinal autofluorescence caused by lysosome-like organelles. The
154 DAPI channel image was subtracted from the green and red channel images to remove
155 autofluorescent signal from the colocalization analysis. The DAPI subtraction was done using
156 the Metamorph "Arithmetic" function at 16-bit depth. Quantification of colocalization
157 (Manders coefficients) in autofluorescence subtracted images was performed using open
158 source Fiji (Image J) software and the "Colocalization Threshold" function. At least 9 animals
159 were used for each analysis. For middle plane images, the fluorescence signal in the apical
160 membrane and the basolateral membrane between two neighboring cells were avoided.

161 **Statistical analysis**

162 Quantified data obtained in this study was graphed and statistically analyzed using GraphPad
163 Prism 7.04 software.

164

165 # Results

166

167 **The SDPN-1 SH3 domain binds to PXF-1 via a specific proline-rich sequence**

168 Syndapin family proteins, also known as PACSINs, contain an N-terminal F-BAR domain (FCH-
169 BAR, Fes/CIP4 homology-Bin/Amphiphysin/Rvs) and a C-terminal SH3 (Src-homology 3) domain
170 (14). *C. elegans* has a single Syndapin family member SDPN-1, while the situation in mammals is
171 more complex, with three Syndapin family members Syndapin1/PACSIN1, Syndapin2/PACSIN2,
172 and Syndapin3/PACSIN3 (26). Syndapins form dimers through their F-BAR domains, with the F-
173 BAR dimer forming a mildly curved structure that binds directly to membrane phospholipids
174 (14). Higher order assemblies of these proteins scaffold the membrane to promote bending and
175 remodeling, in many cases producing membrane tubulation (26). Indeed, our previous work
176 showed that full-length recombinant *C. elegans* SDPN-1 tubulates acidic membranes *in vitro* (9).
177 *In vivo* SDPN-1 localizes to early endosomes and basolateral recycling endosomes in the *C.*
178 *elegans* intestine, and is required for basolateral recycling, but the molecular mechanism(s) by
179 which it mediates endocytic recycling remain poorly understood (9). To gain a better
180 understanding of how SDPN-1 promotes endosomal transport we sought to identify partner
181 proteins that work with SDPN-1 in this process.

182 The SH3 domain is a peptide recognition module for proline-rich sequences that is well-known
183 for mediating specific protein-protein interactions (27). Thus, we focused on the SDPN-1 SH3

184 domain as a molecular entry point to identify direct SDPN-1 binding partners. We were aided in
185 this goal by the *C. elegans* SH3-interactome project (16), a large-scale analysis that used peptide
186 phage display to define the binding preferences for most SH3-domains encoded in the *C.*
187 *elegans* genome, including generating a weighted SDPN-1 SH3 consensus target sequence (Fig.
188 1A). The SH3 interactome project also screened directly for SDPN-1 SH3-domain interacting
189 proteins using a stringent yeast-2-hybrid approach. Importantly, both approaches identified the
190 protein PXF-1 as a prime SDPN-1 SH3 domain candidate. The project recovered PXF-1 via
191 genome-wide yeast-2-hybrid with a SDPN-1 SH3 bait, but not any of the other SH3 domain
192 baits, and independently identified PXF-1 amino acids 191-198 as the second-best match for
193 the SDPN-1 SH3-binding consensus in the entire predicted *C. elegans* proteome (16).

194 PXF-1 (PDZ-GEF or RAGEF in mammals) is a well-characterized exchange factor for the small
195 Ras-like GTPases RAP-1/Rap1 and RAP-2/Rap2, and Rap-GTPases have been implicated in some
196 endocytic recycling events in other organisms, further suggesting that a SDPN-1/PXF-1
197 interaction could be relevant to understanding the role of SDPN-1 in recycling (17, 28-30). PXF-1
198 has a complex domain structure, with two RCBD-like domains: one near the N-terminus, and
199 the other more centrally located(17, 31). While RCBD domains in some proteins bind to cAMP,
200 biochemical analysis of human PDZ-GEF2, a PXF-1 ortholog, failed to identify any cyclic-
201 nucleotide binding for these RCBD-like domains (32). The predicted SDPN-1 SH3 binding site at
202 residues 191-198 resides in a predicted unstructured region between the two RCBD-like
203 domains (https://alphafold.ebi.ac.uk/entry/G5EDB9). PXF-1 also contains REM (Ras Exchange
204 Motif), PDZ (PSD-95, Dlg, and ZO-1 homology), RA (Ras Association), and GEF (Guanine

205 nucleotide Exchange Factor) domains, as well as a C-terminal VSRV sequence that may interact
206 with PDZ-domains (Fig 1B) (17).
207
208 To better analyze the ability of the SDPN-1 SH3 domain to bind to PXF-1, and test the
209 importance of the predicted binding site identified as a strong match to the phage-display
210 consensus sequence, we performed GST pulldown experiments. As baits we compared GST,
211 GST-SH3^{sdpn-1}(+), and GST-SH3^{sdpn-1}(P478L). The P478L mutation in the SDPN-1 SH3 domain is
212 equivalent to mammalian Syndapin I P434L, which was previously shown to abolish the ability
213 of the Syndapin I SH3 domain to bind partner proteins (33). These baits were paired with *in*
214 *vitro* translated HA-PXF-1(1-478) bearing the wild-type sequence, or with the consensus-
215 matching PXF-1(191-198) SH3 binding site mutated (**K**GPA**P**LP**P** to **A**GPA**A**LP**A**) (Fig 1A-B). We
216 found that HA-PXF-1(+) interacted robustly with GST-SH3^{sdpn-1}(+), but not GST or GST-SH3^{sdpn-}
217 ^{1}(P478L), indicating the specificity of the interaction. Moreover, we found that mutation of HA-
218 PXF-1 at the predicted interaction sequence (191-198) abolished the interaction with GST-
219 SH3^{sdpn-1}(+), despite other proline-rich sequences remaining in the PXF-1 prey protein. Taken
220 together these results indicate that the SDPN-1 SH3 domain can bind to PXF-1, and the
221 predicted binding site at aa191-198 is crucial for this interaction.
222
223 **The SDPN-1/PXF-1 interaction is important for endocytic recycling**

224 Given our binding results we hypothesized that the interaction of the SDPN-1 SH3-domain with
225 PXF-1 is important for SDPN-1-mediated regulation of endocytic recycling. To interfere with this
226 interaction *in vivo* we used CRISPR-mediated genome editing to create *C. elegans* mutants

227 *sdpn-1(pw33)* and *pxf-1(pw34)*, in which the same point mutations that interfered with the
228 SDPN-1/PXF-1 binding interaction *in vitro* were engineered into the endogenous *sdpn-1* and
229 *pxf-1* genes *in vivo* (Fig. 1b). While *pxf-1* null mutations are lethal (17), *pxf-1(pw34)* is a viable
230 allele.

231 In particular we found that the interaction-defective mutants *sdpn-1(pw33)* and *pxf-1(pw34)*
232 displayed gross over-accumulation of intestinal GFP::RME-1 marked basolateral recycling
233 endosomes and GFP::RAB-5 marked early endosomes in the central cytoplasm (middle plane
234 Fig. 2K), very similar to phenotypes we had previously observed in null mutants for *sdpn-1* (Fig.
235 2, panel A-A'' and B-B''; Fig. S1 A, A") (9). For GFP::RME-1 labeled recycling endosomes we
236 measured endosome fluorescence intensity and number. In the case of GFP::RAB-5, the
237 mutants accumulated so many early endosomal compartments that it was not possible to
238 segment the images to quantify endosome number, so in addition to fluorescence intensity we
239 measured the the percent of total cytoplasmic area labeled by GFP::RAB-5.

240 We also tested the importance of the SDPN-1/PXF-1 interaction in cargo trafficking, focused on
241 well-characterized model endocytic recycling cargoes markers hTAC (human IL2-receptor alpha-
242 chain) and hTFR (human transferrin receptor) tagged with GFP, both of which depend upon
243 SDPN-1 for their recycling (9, 10). hTAC is a clathrin-independent cargo that recycles via the
244 recycling endosome in an ARF-6-dependent pathway (34, 35), while hTFR is clathrin-dependent
245 in its endocytosis and also recycles via recycling endosomes (10). Previous studies showed that
246 *sdpn-1* null mutants display dramatic endosomal accumulation of hTAC and hTFR within the
247 intestinal cells (9). Importantly, we observed that the interaction-defective mutants caused

248 intracellular accumulation of recycling cargoes similar to that previously observed upon the
249 complete loss of SDPN-1 (Fig. 2, panel C-C'' and D-D''). Taken together, our results indicate that
250 a SDPN-1/PXF-1 interaction is important for the function of the basolateral recycling pathway.

251

252 **The RAP-1 GTPase cycle is required for endocytic recycling**

253 Since *C. elegans* PXF-1 and its mammalian homologs are specific GDP/GTP exchange factors for
254 Rap-GTPases *in vivo* and *in vitro* (17, 36, 37), we surmised that the role of the SDPN-1/PXF-1
255 interaction is to activate Rap-GTPases to promote endocytic recycling. To test this hypothesis,
256 we analyzed the effect of a *rap-1(0)* mutant on relevant markers *in vivo*. Indeed, we found that
257 *rap-1* null mutants displayed significantly increased accumulation of RAB-5 marked early
258 endosomes and RME-1 marked recycling endosomes, as well as increased intracellular
259 accumulation of recycling cargo markers hTAC::GFP and hTFR::GFP, supporting this hypothesis
260 (Fig. 2, panel A''', B''', C''', D''', F, H-J; Fig. S1 A, A"). Interestingly, we also identified abnormal
261 accumulation defects for recycling cargo and endosome markers in a GTPase-defective *rap-*
262 *1(re180*) mutant (38), bearing the G12V mutation at the endogenous gene (Fig. 2B',C'''', D'''',
263 E'''', F, G, I-J; Fig. S1 A'). These results indicate a requirement for the full RAP-1 GTP/GDP-cycle,
264 rather than a simple requirement for active RAP-1. We also tested for effects of *sdpn-1(0)* and
265 *rap-1(0)* mutants on GFP-tagged *C. elegans* GLUT1 homolog FGT-1, a glucose transporter known
266 to be naturally expressed in the *C. elegans* intestine (39). Loss of SDPN-1 and RAP-1 produced
267 similar intracellular retention of FGT-1::GFP, also suggesting a defect in recycling (Fig. S2). Taken
268 together these results support an important role for RAP-1 in regulating recycling downstream
269 of SDPN-1 and PXF-1.

270

271 **PXF-1 and RAP-1 are enriched on early and basolateral recycling endosomes**

272 To further interrogate SDPN-1, PXF-1, and RAP-1 for shared function together in recycling, we
273 compared the localization of PXF-1 and RAP-1 with SDPN-1 in the context of the intestinal
274 epithelium within the intact whole animal. We also compared RAP-1 localization to
275 independent early endosome and basolateral recycling endosome markers with which SDPN-1
276 is known to colocalize (9). We found that endogenously tagged PXF-1::GFP colocalized with
277 intestinal SDPN-1::tagRFP indicating significant residence of PXF-1 with SDPN-1 on basolateral
278 endosomes (Fig 3 A-A''''and E). We also identified strong colocalization of intestinal SDPN-
279 1::GFP with tagRFP::RAP-1, indicating that at any given time most SDPN-1 overlaps with RAP-1
280 on the same endosomes (Fig 3 B-B''''and E). We did note that RAP-1 distribution appeared
281 broader than that of SDPN-1, as reflected in a lesser but still substantial Manders' coefficient
282 for the reverse comparison (Fig 3E). RAP-1 labeling of structures that were SDPN-1-negative
283 could reflect endosomal microdomains lacking SDPN-1, and/or additional RAP-1 positive
284 organelle types such as late endosomes (40). We also observed considerable overlap between
285 tagRFP::RAP-1 and basolateral recycling endosome marker GFP::RME-1 (Fig 3C-C'''), and early
286 endosome marker GFP::RAB-5 (Fig 3D-D'''), further supporting the interpretation that SDPN-1
287 and RAP-1 are present on the same early and basolateral recycling endosomes where they
288 could function together to regulate endocytic recycling.

289

290 **RHO-1 is enriched on SDPN-1 and RAP-1 positive endosomes**

291 Given our findings indicating that RAP-1 signaling functions downstream of SDPN-1 to promote
292 recycling, we sought to better understand the relevant target of RAP-1 for this process. While
293 previous studies of Rap-GTPases had not identified a target of Rap-signaling for regulation of
294 recycling, some reports indicated that mammalian Rap1 or Rap2 can negatively regulate RhoA
295 to promote mammalian epithelial cell spreading, endothelial barrier function, or ECM stiffness
296 mechanotransduction, in part via ARHGAP29 (41-45). We hypothesized that misregulation of
297 endosomal Rho-GTPase activity could explain *sdpn-1/pxf-1/rap-1* associated phenotypes.
298 Supporting this notion, we found that mutation of *spv-1*, the closest *C. elegans* homolog of
299 ARFGAP29, resulted in an increase in RME-1 labeled recycling endosome number, similar to the
300 defect displayed in *pxf-1* and *rap-1* mutants (Fig. S3).

301 Given these results, we tested for a role of SDPN-1 and RAP-1 in the regulation of endosomal
302 RHO-1, the only *C. elegans* homolog of RhoA (46). First, we assayed for enrichment of RHO-1 on
303 the relevant endosomes in the *C. elegans* intestine, the expected location for direct function as
304 part of the basolateral recycling pathway. Indeed we found that nearly all SDPN-1::GFP positive
305 structures contained tagRFP::RHO-1 (Fig 4 A-A'''' and 4C), while tagRFP::RHO-1 was also present
306 on SDPN-1 negative structures (Fig 4 A-A'''' and 4C). Importantly, GFP::RHO-1 and tagRFP::RAP-
307 1 colocalized very well, with most endosomes positive for one also positive for the other (Fig.4
308 B-B''' and 4C). Taken together, these results indicate that RHO-1 is enriched on the same
309 endosomes as SDPN-1 and RAP-1, pointing to the potential for a SDPN-1/PXF-1/RAP-1 module
310 influencing endosomal RHO-1 activity.

311

312 **SDPN-1 and RAP-1 negatively regulate RHO-1**

313 If RHO-1 is regulated by SDPN-1 and RAP-1, we might expect to find a change in RHO-1
314 subcellular localization in *sdpn-1* and *rap-1* mutants. Indeed, we found an increased
315 accumulation of GFP::RHO-1 in intracellular puncta in both mutants (Figure S4). This result was
316 suggestive, but was not sufficient to define any changes in RHO-1 GTP-level.

317 To directly test for effects of *sdpn-1* and *rap-1* mutants on intestinal endosomal RHO-1
318 activation state, we co-expressed a RHO-1(GTP) biosensor (GFP::AHPH) (47) with tagRFP::RHO-
319 1, assaying for changes in GFP::AHPH recruitment to tagRFP::RHO-1 labeled endosomes in the
320 intestine. If SDPN-1 normally acts to negatively regulate RHO-1 activation via RAP-1 signaling,
321 we would expect *sdpn-1* and *rap-1* mutants to show increased RHO-1 activation, leading to
322 increased GFP::AHPH recruitment. Indeed, we measured a significant increase in the
323 colocalization of RHO-1 and its active-state biosensor on intracellular structures in *sdpn-1* or
324 *rap-1* null mutant backgrounds, indicating abnormally high RHO-1(GTP) levels on intestinal
325 endosomes (Fig. 4D-G). Importantly, there was no change in GFP::AHPH colocalization and
326 tagRFP::RHO-1 on the apical plasma membrane, indicating the specificity of this regulation (Fig
327 4H). This data suggests a model in which a critical function of the SDPN-1/PXF-1/RAP-1 pathway
328 is to prevent the inappropriate overactivation of RHO-1 on endosomes that could interfere with
329 recycling function.

330 **RHO-1 functions downstream of SDPN-1 to regulate endocytic recycling**

331 A corollary to this model is that reducing RHO-1 levels could be expected to compensate for
332 elevated RHO-1 activation in *sdpn-1* mutants, leading to rescue of *sdpn-1* endocytic recycling

333 defects. To test this hypothesis directly, we used RNAi to deplete RHO-1 in a *sdpn-1* mutant
334 background and assayed for effects on recycling endosomes and endocytic recycling cargo.
335 Since *rho-1* is an essential gene, we established RNAi conditions that strongly depleted RHO-1,
336 as verified in a tagRFP::RHO-1 strain (Fig. S5), but allowed development to the adult stage
337 typically used in our assays. Remarkably, this RNAi-mediated depletion of RHO-1 fully
338 suppressed *sdpn-1* null mutant defects that normally result in abnormal accumulation of
339 GFP::RME-1-labeled recycling endosomes and hTAC::GFP recycling cargo (Fig. 6, panel A-B'''').
340 These results strongly support regulation of endosomal RHO-1 as a key factor in the SDPN-1-
341 dependent regulation of endocytic recycling.

342 **Non-muscle myosin II is a key regulator of recycling downstream of SDPN-1, RAP-1 and RHO-1**

343 Given our results with RHO-1, we sought greater insight into which RHO-1-mediated activities
344 influence recycling. *C. elegans* RHO-1 and mammalian RhoA are well known for regulating
345 actomyosin contractility through non-muscle myosin II (48, 49). In support of a roll for myosin II
346 in this pathway, we found that SDPN-1 colocalized with MLC-4, the myosin II regulatory light
347 chain reported to function with non-muscle myosin II heavy chain isoforms NMY-1 and NMY-2
348 (Fig. 4, panel C-C''' and D). We also found that loss of SDPN-1 increased intracellular
349 accumulation of punctate MLC-4 intracellular signal suggesting increased recruitment to
350 endosomal membranes (50).

351 If regulation of myosin II contraction cycling is a key output of SDPN-1/PXF-1/RAP-1 signaling
352 for endocytic recycling, forced activation of myosin II activity might be expected interfere with
353 endosome function. Indeed, we found that forced activation of non-muscle myosin II in the

354 intestine via expression of a constitutively active phosphomimetic form of MLC-4 (MLC-4(DD))
355 (50), increased intracellular retention of recycling cargo hTAC::GFP, and resulted in intracellular
356 accumulation of RAB-5 and RME-1 marked endosomes (Fig. 6, panel E-H; Fig S1C'-C''). These
357 results support a requirement for myosin II regulation on endosomes for successful endocytic
358 recycling.

359 To investigate myosin II requirements further, we assayed for effects of depletion of non-
360 muscle myosin II isoforms NMY-1 and NMY-2. Importantly, depletion of myosin II isoform NMY-
361 2 caused intracellular accumulation of recycling endosome marker RME-1 and recycling cargo
362 hTAC::GFP similar to *sdpn-1* mutants, while depletion of NMY-1 did not (Fig 7 H-J, G). By
363 contrast, depletion of myosin II isoform NMY-1, but not depletion of NMY-2, strongly
364 suppressed *sdpn-1* null mutant intracellular accumulation of GFP::RME-1-labeled recycling
365 endosomes and recycling cargo hTAC::GFP, similar to the effects of RHO-1 depletion (Fig. 7).
366 Taken together these results strongly support a key role for myosin II regulation on endosomes
367 in recycling function, with NMY-1 as a likely target of SDPN-1/PXF-1/RAP-1/RHO-1 regulation
368 (Fig.8).

369

370 **Discussion**

371 Syndapin/PACSIN proteins have long been implicated in endocytic recycling in multiple
372 organisms, but a clear understanding of the mechanism of action of these proteins in
373 endosomal regulation has remained unclear (Braun et al., 2005; Farmer et al., 2021; Gleason et

374 al., 2016). Some clues are provided by the syndapin/PACSIN domain organization that is
375 characterized by a single N-terminal F-BAR domain that links these proteins to membranes, and
376 a single C-terminal SH3 domain that interacts with other proteins. Our new *in vivo* data
377 reinforces the essential nature of the SH3 domain to syndapin/PACSIN function in recycling,
378 finding that a point mutation in the SH3 domain of endogenous *sdpn-1* produced endocytic
379 recycling defects in the *C. elegans* intestine equivalent to those we previously established for
380 *sdpn-1* null mutants. Thus, identifying the key physiologically relevant binding partners of the
381 SDPN-1 SH3 domain is essential to understanding how SDPN-1 controls recycling.

382 The *C. elegans* SH3-ome project predicted a high likelihood binding site for the SDPN-1 SH3 in
383 RAP-GEF PXF-1, an interaction that we confirmed biochemically. We found the importance of
384 the interaction *in vivo* to be clear, as mutation of this binding site in endogenous *pxf-1* also
385 severely impaired endocytic recycling, causing intracellular accumulation of intestinal
386 basolateral recycling cargo and abnormal accumulation of markers of early and basolateral
387 recycling endosomes. The role of PXF-1 in recycling appears to match its known biochemical
388 activity as a Rap-GEF, as our results further showed that loss of PXF-1 target RAP-1 also
389 impaired intestinal recycling, and PXF-1 and RAP-1 are enriched on SDPN-1 labeled endosomes
390 as would be expected if they function together. Although Rap GTPases have not been well
391 studied in the context of recycling, mammalian Rap1 and Rap2 have been reported to be
392 enriched on recycling endosomes, with Rap1 supporting recycling of the GABA(B) receptor in
393 neurons, and Rap2 supporting recycling of integrin LFA-1 in T lymphocytes (28, 51). Taken
394 together with our data in *C. elegans* we conclude that a requirement for Rap-GTPases in
395 endocytic recycling is evolutionarily conserved. Thus, gaining insight into how Rap GTPases are

396 regulated on recycling endosomes, and understanding the mechanisms by which Rap activation
397 influences recycling function in *C. elegans* should be broadly applicable to other organisms, and
398 has important implications for higher order processes known to require Rap signaling, including
399 cell adhesion, cell migration, cell polarity, and cell fate specification.

400 What then is the function of RAP-1 signaling from endosomes during recycling? One known
401 output of Rap signaling is the negative regulation of RhoA, a function first shown during neurite
402 outgrowth, and also prominent during endothelial barrier formation (41, 52). Indeed, we found
403 that *C. elegans* RHO-1/RhoA was highly enriched on early and basolateral recycling endosomes
404 in the adult *C. elegans* intestine, and RHO-1 activation was increased upon loss of SDPN-1 or
405 RAP-1 as judged by a RHO-1(GTP) biosensor, indicating that SDPN-1 and RAP-1 act as negative
406 regulators of RHO-1 activity on endosomes. Importantly, our results further revealed RHO-1
407 negative regulation as a key output of SDPN-1 signaling relevant to recycling, since a reduction
408 in RHO-1 levels by RNAi strongly suppressed the recycling defects of *sdpn-1* mutants. We note
409 that recent work in mammalian epithelial cells found cortical recycling endosomes as a major
410 site of RhoA activation, in this case relevant to stress fiber generation and front-rear polarity
411 acquisition, although this work did not test for effects of RhoA activation on recycling function
412 (53). These similarities further suggest that our findings will be relevant in a broad context
413 across species.

414 We further sought to determine which output of RHO-1 signaling was most relevant to SDPN-1-
415 mediated recycling regulation. RhoA is a well-established regulator of actomyosin contractility
416 that functions through effectors mDia1 (a diaphanous-related formin) and ROCK (Rho-

417 associated serine/threonine kinase), with ROCK activating non-muscle myosin II and actin
418 dynamics (48). Our experiments found that depletion of the NMY-1 isoform of non-muscle
419 myosin II was sufficient to significantly suppress *sdpn-1* mutant defects. These results indicate
420 that inappropriately high levels of active myosin II, or the inability to move through complete
421 myosin contractility cycles, explains at least part of the effects of *sdpn-1* mutants on recycling
422 (Gleason et al., 2016; Yan et al., 2021). This interpretation is supported by our results showing
423 that constitutive activation of myosin II by expression of a myosin light chain phosphomimetic
424 also impairs recycling function, and our findings that myosin light chain is enriched on SDPN-1
425 positive endosomes.

426 Surprisingly, we found the opposite phenotype for non-muscle myosin isoform NMY-2.
427 Depletion of NMY-2 caused intracellular accumulation of recycling cargo, indicating a positive
428 role for NMY-2 in recycling. Interestingly, previous work on NMY-1 and NMY-2 documented
429 opposing effects in the regulation of the contractile ring channels of the *C. elegans* gonad (22).
430 Mathematical modeling in that work suggested that these opposing effects could be explained
431 by NMY-1 and NMY-2 contractile fibers exerting forces in opposing directions, one normal to
432 the ring, and the other tangential (22). If these principles apply to the recycling endosome case,
433 NMY-2 derived forces might increase tension on endosomal tubules to promote their fission,
434 while NMY-1 contraction in an opposing direction might reduce tubule tension and fission.
435 Normal recycling tubule release might require cycles of increased and decreased tension, or
436 forces regulating recycling rates might be modulated in response to changes in cellular
437 requirements, such as changes in cargo load or metabolism.

438 Interestingly, three putative Rho effectors, formin CYK-1/mDia, LET-502/ROCK, and RTKN-
439 1/Rhotekin, are known to function in basolateral recycling in the *C. elegans* intestine, although
440 current models posit that these proteins function independently of RHO-1 in recycling (11, 54,
441 55). Branched actin formed by Arp2/3 is traditionally considered the relevant F-actin type
442 associated with endosomes, but recycling may require a balance of branched and linear actin
443 for proper function. Actin tracks produced by CYK-1 could be substrates upon which cycles of
444 myosin II contractility would act, potentially producing cycles of actomyosin-driven endosomal
445 membrane tension that could promote cycles of tubular cargo carrier fission.

446 We note that non-muscle myosin II was previously shown to promote mitochondrial fission and
447 could contribute to endosomal fission during recycling in a similar way (56-59). Myosin II,
448 Spire1C, and endoplasmic reticulum-bound formin INF2 have been proposed to create
449 actomyosin tension that deforms the outer mitochondrial membrane during "prefission",
450 promoting curvature-sensing-based recruitment of dynamin-related protein Drp1 and other
451 factors that complete mitochondrial constriction (59). Further work will be required to
452 determine if a similar process is operative at the early endosome – recycling endosome
453 interface, and if there is a relationship between SDPN-1/RAP-1/RHO-1/NMY-1 and previously
454 identified functions for LET-502/RTKN-1/CYK-1 during recycling.

455 Syndapin/PACSIN proteins are often thought of as acting directly in endosomal tubule
456 generation or tubule severing, since isolated BAR domains from several of these proteins are
457 able to generate tubules from liposomes *in vitro*, and in some cases enhance endosomal
458 tubulation when overexpressed *in vivo*. However, it remains unclear if an F-BAR-driven

459 constricting/tubulating activity is a key output of syndapin/PACSINs that promotes recycling
460 function. An alternate hypothesis is that the key function of the F-BAR domain in
461 syndapin/PACSINs is to provide membrane binding and curvature-sensing that brings
462 syndapin/PACSIN to endosomal tubules elaborated by other means, such as cytoskeletal
463 pushing and pulling forces. In the *C. elegans* intestine and human HeLa cells RAB-10/Rab10 is
464 essential for the extensive tubulation found in the recycling endosome network (10, 60-64). In
465 the *C. elegans* case microfilament and microtubule integrity is required for network structure,
466 and RAB-10 is known to regulate association of endosomal membranes with actin filaments via
467 the EHBP-1 protein (60, 63, 64). In the HeLa case Rab10-mediated regulation of Kif13/kinesin
468 pulling forces have also been implicated (61).

469 Our new data clearly points to an essential role for Syndapin in signaling via Rap and Rho to
470 control myosin II on endosomes (Fig.8), but we cannot rule out an additional mechanical
471 contribution of SDPN-1 to endosomal function via direct membrane bending. However, the high
472 efficiency of *sdpn-1* mutant recycling phenotype suppression by *rho-1* depletion suggests that
473 RHO-1 regulation is the main output relevant to recycling. We also note that in some systems
474 syndapin/PACSIN proteins associate with other trafficking regulators such as MICAL-L1, OCRL1,
475 Dynamin, and EHD1/RME-1 that could promote tubulation and/or severing (62). It will be of
476 great interest to revisit the question of relative contributions to the tubule-based recycling
477 mechanism as new genetic and cell biological tools evolve, allowing more complete, acute, and
478 fine-tuned control of experimental conditions, as we further elaborate our understanding of
479 this complex system.

480

481 ## Acknowledgments

482 We would like to thank the Grant lab for critical comments and suggestions. We thank Peter
483 Schweinsberg and Ge Bai for technical assistance in making plasmid clones and biolistic
484 transgenic lines, and Helen Ushakov for expert microinjection. We thank Adriana Dawes for
485 *nmy-1* and *nmy-2* RNAi clones, Michel Labouesse for *mlc-4* wild-type and phosphomimetic DNA
486 clones, and David Reiner for *rap-1* mutant strains. We also thank Michael Pierce, Noriko
487 Goldsmith and Jessica Shivas for help with confocal microscopy, and Gary Bader for SH3
488 weighted match analysis. This work was supported by NIH Grant 5R01GM135326 to B.D.G.

489

490 ## References

491 1. G. J. Doherty, H. T. McMahon, Mechanisms of endocytosis. *Annu Rev Biochem* **78**, 857-902
492 (2009).
493 2. L. Maldonado-Báez, C. Williamson, J. G. Donaldson, Clathrin-independent endocytosis: a cargo-
494 centric view. *Exp Cell Res* **319**, 2759-2769 (2013).
495 3. J. A. Solinger, A. Spang, Sorting of cargo in the tubular endosomal network. *Bioessays* **44**,
496 e2200158 (2022).
497 4. B. D. Grant, J. G. Donaldson, Pathways and mechanisms of endocytic recycling. *Nat Rev Mol Cell*
498 *Biol* **10**, 597-608 (2009).
499 5. J. D. McGhee, The C. elegans intestine. *WormBook* 10.1895/wormbook.1.133.1, 1-36 (2007).

500 6. B. Leung, G. J. Hermann, J. R. Priess, Organogenesis of the Caenorhabditis elegans intestine. *Dev*
501 *Biol* **216**, 114-134 (1999).
502 7. B. Grant *et al.*, Evidence that RME-1, a conserved C. elegans EH-domain protein, functions in
503 endocytic recycling. *Nat Cell Biol* **3**, 573-579 (2001).
504 8. K. Sato, A. Norris, M. Sato, B. D. Grant, C. elegans as a model for membrane traffic. *WormBook*
505 10.1895/wormbook.1.77.2, 1-47 (2014).
506 9. A. M. Gleason, K. C. Nguyen, D. H. Hall, B. D. Grant, Syndapin/SDPN-1 is required for endocytic
507 recycling and endosomal actin association in the C. elegans intestine. *Mol Biol Cell* **27**, 3746-
508 3756 (2016).
509 10. C. C. Chen *et al.*, RAB-10 is required for endocytic recycling in the Caenorhabditis elegans
510 intestine. *Mol Biol Cell* **17**, 1286-1297 (2006).
511 11. Y. Yan *et al.*, RTKN-1/Rhotekin shields endosome-associated F-actin from disassembly to ensure
512 endocytic recycling. *J Cell Biol* **220** (2021).
513 12. E. Casal *et al.*, The crystal structure of the BAR domain from human Bin1/amphiphysin II and its
514 implications for molecular recognition. *Biochemistry* **45**, 12917-12928 (2006).
515 13. A. Braun *et al.*, EHD proteins associate with syndapin I and II and such interactions play a crucial
516 role in endosomal recycling. *Mol Biol Cell* **16**, 3642-3658 (2005).
517 14. A. Quan, P. J. Robinson, Syndapin--a membrane remodelling and endocytic F-BAR protein. *Febs j*
518 **280**, 5198-5212 (2013).
519 15. J. Kovár, Hybridoma cultivation in defined serum-free media: growth-supporting substances. II.
520 Insulin, other hormones, and growth factors. *Folia Biol (Praha)* **32**, 304-310 (1986).
521 16. X. Xin *et al.*, SH3 interactome conserves general function over specific form. *Mol Syst Biol* **9**, 652
522 (2013).

523 17. W. Pellis-van Berkel *et al.*, Requirement of the Caenorhabditis elegans RapGEF pxf-1 and rap-1
524 for epithelial integrity. *Mol Biol Cell* **16**, 106-116 (2005).
525 18. M. R. Kooistra, N. Dubé, J. L. Bos, Rap1: a key regulator in cell-cell junction formation. *J Cell Sci*
526 **120**, 17-22 (2007).
527 19. C. Frøkjær-Jensen *et al.*, Random and targeted transgene insertion in Caenorhabditis elegans
528 using a modified Mos1 transposon. *Nat Methods* **11**, 529-534 (2014).
529 20. L. Timmons, A. Fire, Specific interference by ingested dsRNA. *Nature* **395**, 854 (1998).
530 21. R. S. Kamath, J. Ahringer, Genome-wide RNAi screening in Caenorhabditis elegans. *Methods* **30**,
531 313-321 (2003).
532 22. V. C. Coffman, T. M. Kachur, D. B. Pilgrim, A. T. Dawes, Antagonistic Behaviors of NMY-1 and
533 NMY-2 Maintain Ring Channels in the C. elegans Gonad. *Biophys J* **111**, 2202-2213 (2016).
534 23. A. Paix, A. Folkmann, G. Seydoux, Precision genome editing using CRISPR-Cas9 and linear repair
535 templates in C. elegans. *Methods* **121-122**, 86-93 (2017).
536 24. G. Huang *et al.*, Improved CRISPR/Cas9 knock-in efficiency via the self-excising cassette (SEC)
537 selection method in C. elegans. *MicroPubl Biol* **2021** (2021).
538 25. M. L. Schwartz, M. W. Davis, M. S. Rich, E. M. Jorgensen, High-efficiency CRISPR gene editing in
539 C. elegans using Cas9 integrated into the genome. *PLoS Genet* **17**, e1009755 (2021).
540 26. Q. Wang *et al.*, Molecular mechanism of membrane constriction and tubulation mediated by the
541 F-BAR protein Pacsin/Syndapin. *Proc Natl Acad Sci U S A* **106**, 12700-12705 (2009).
542 27. H. Meng *et al.*, PACSIN 2 represses cellular migration through direct association with cyclin D1
543 but not its alternate splice form cyclin D1b. *Cell Cycle* **10**, 73-81 (2011).
544 28. P. Stanley, S. Tooze, N. Hogg, A role for Rap2 in recycling the extended conformation of LFA-1
545 during T cell migration. *Biol Open* **1**, 1161-1168 (2012).

546 29. F. Balzac *et al.*, E-cadherin endocytosis regulates the activity of Rap1: a traffic light GTPase at the
547 crossroads between cadherin and integrin function. *J Cell Sci* **118**, 4765-4783 (2005).
548 30. L. Li *et al.*, A unique interplay between Rap1 and E-cadherin in the endocytic pathway regulates
549 self-renewal of human embryonic stem cells. *Stem Cells* **28**, 247-257 (2010).
550 31. Y. Liao *et al.*, RA-GEF, a novel Rap1A guanine nucleotide exchange factor containing a
551 Ras/Rap1A-associating domain, is conserved between nematode and humans. *J Biol Chem* **274**,
552 37815-37820 (1999).
553 32. H. B. Kuiperij *et al.*, Characterisation of PDZ-GEFs, a family of guanine nucleotide exchange
554 factors specific for Rap1 and Rap2. *Biochim Biophys Acta* **1593**, 141-149 (2003).
555 33. B. Qualmann, J. Roos, P. J. DiGregorio, R. B. Kelly, Syndapin I, a synaptic dynamin-binding protein
556 that associates with the neural Wiskott-Aldrich syndrome protein. *Mol Biol Cell* **10**, 501-513
557 (1999).
558 34. A. Shi *et al.*, RAB-10-GTPase-mediated regulation of endosomal phosphatidylinositol-4,5-
559 bisphosphate. *Proc Natl Acad Sci U S A* **109**, E2306-2315 (2012).
560 35. R. J. Gleason, A. M. Akintobi, B. D. Grant, R. W. Padgett, BMP signaling requires retromer-
561 dependent recycling of the type I receptor. *Proc Natl Acad Sci U S A* **111**, 2578-2583 (2014).
562 36. E. W. Frische *et al.*, RAP-1 and the RAL-1/exocyst pathway coordinate hypodermal cell
563 organization in Caenorhabditis elegans. *Embo j* **26**, 5083-5092 (2007).
564 37. J. F. Rebhun, A. F. Castro, L. A. Quilliam, Identification of guanine nucleotide exchange factors
565 (GEFs) for the Rap1 GTPase. Regulation of MR-GEF by M-Ras-GTP interaction. *J Biol Chem* **275**,
566 34901-34908 (2000).
567 38. N. R. Rasmussen, D. J. Dickinson, D. J. Reiner, Ras-Dependent Cell Fate Decisions Are Reinforced
568 by the RAP-1 Small GTPase in Caenorhabditiselegans. *Genetics* **210**, 1339-1354 (2018).

569 39. Y. Feng, B. G. Williams, F. Koumanov, A. J. Wolstenholme, G. D. Holman, FGT-1 is the major
570 glucose transporter in C. elegans and is central to aging pathways. *Biochem J* **456**, 219-229
571 (2013).
572 40. V. Pizon, M. Desjardins, C. Bucci, R. G. Parton, M. Zerial, Association of Rap1a and Rap1b
573 proteins with late endocytic/phagocytic compartments and Rap2a with the Golgi complex. *J Cell*
574 *Sci* **107 (Pt 6)**, 1661-1670 (1994).
575 41. A. Post, W. J. Pannekoek, B. Ponsioen, M. J. Vliem, J. L. Bos, Rap1 Spatially Controls ArhGAP29 To
576 Inhibit Rho Signaling during Endothelial Barrier Regulation. *Mol Cell Biol* **35**, 2495-2502 (2015).
577 42. A. Post *et al.*, Rasip1 mediates Rap1 regulation of Rho in endothelial barrier function through
578 ArhGAP29. *Proc Natl Acad Sci U S A* **110**, 11427-11432 (2013).
579 43. G. A. Smolen *et al.*, A Rap GTPase interactor, RADIL, mediates migration of neural crest
580 precursors. *Genes Dev* **21**, 2131-2136 (2007).
581 44. C. W. Wilson *et al.*, Rasip1 regulates vertebrate vascular endothelial junction stability through
582 Epac1-Rap1 signaling. *Blood* **122**, 3678-3690 (2013).
583 45. Z. Meng *et al.*, RAP2 mediates mechanoresponses of the Hippo pathway. *Nature* **560**, 655-660
584 (2018).
585 46. B. Saenz-Narciso, E. Gomez-Orte, A. Zheleva, I. Gastaca, J. Cabello, Control of developmental
586 networks by Rac/Rho small GTPases: How cytoskeletal changes during embryogenesis are
587 orchestrated. *Bioessays* **38**, 1246-1254 (2016).
588 47. Y. C. Tse *et al.*, RhoA activation during polarization and cytokinesis of the early Caenorhabditis
589 elegans embryo is differentially dependent on NOP-1 and CYK-4. *Mol Biol Cell* **23**, 4020-4031
590 (2012).
591 48. M. Chircop, Rho GTPases as regulators of mitosis and cytokinesis in mammalian cells. *Small*
592 *GTPases* **5** (2014).

593 49. B. Sáenz-Narciso, E. Gómez-Orte, A. Zheleva, I. Gastaca, J. Cabello, Control of developmental
594 networks by Rac/Rho small GTPases: How cytoskeletal changes during embryogenesis are
595 orchestrated. *Bioessays* **38**, 1246-1254 (2016).
596 50. C. Gally *et al.*, Myosin II regulation during C. elegans embryonic elongation: LET-502/ROCK,
597 MRCK-1 and PAK-1, three kinases with different roles. *Development* **136**, 3109-3119 (2009).
598 51. Z. Zhang *et al.*, GABAB receptor promotes its own surface expression by recruiting a Rap1-
599 dependent signaling cascade. *J Cell Sci* **128**, 2302-2313 (2015).
600 52. T. Yamada, T. Sakisaka, S. Hisata, T. Baba, Y. Takai, RA-RhoGAP, Rap-activated Rho GTPase-
601 activating protein implicated in neurite outgrowth through Rho. *J Biol Chem* **280**, 33026-33034
602 (2005).
603 53. C. Gaston *et al.*, EpCAM promotes endosomal modulation of the cortical RhoA zone for
604 epithelial organization. *Nat Commun* **12**, 2226 (2021).
605 54. T. Gong *et al.*, PTRN-1/CAMSAP promotes CYK-1/formin-dependent actin polymerization during
606 endocytic recycling. *Embo j* **37** (2018).
607 55. W. Zhang *et al.*, LET-502/ROCK Regulates Endocytic Recycling by Promoting Activation of RAB-5
608 in a Distinct Subpopulation of Sorting Endosomes. *Cell Rep* **32**, 108173 (2020).
609 56. F. Korobova, T. J. Gauvin, H. N. Higgs, A role for myosin II in mammalian mitochondrial fission.
610 *Curr Biol* **24**, 409-414 (2014).
611 57. U. Manor *et al.*, A mitochondria-anchored isoform of the actin-nucleating spire protein regulates
612 mitochondrial division. *Elife* **4** (2015).
613 58. A. L. Hatch, P. S. Gurel, H. N. Higgs, Novel roles for actin in mitochondrial fission. *J Cell Sci* **127**,
614 4549-4560 (2014).
615 59. C. Yang, T. M. Svitkina, Ultrastructure and dynamics of the actin-myosin II cytoskeleton during
616 mitochondrial fission. *Nat Cell Biol* **21**, 603-613 (2019).

617 60. A. Shi *et al.*, EHBP-1 functions with RAB-10 during endocytic recycling in Caenorhabditis elegans.
618 *Mol Biol Cell* **21**, 2930-2943 (2010).
619 61. K. Etoh, M. Fukuda, Rab10 regulates tubular endosome formation through KIF13A and KIF13B
620 motors. *J Cell Sci* **132** (2019).
621 62. T. Farmer *et al.*, Defining the protein and lipid constituents of tubular recycling endosomes. *J*
622 *Biol Chem* **296**, 100190 (2021).
623 63. P. Wang *et al.*, RAB-10 Promotes EHBP-1 Bridging of Filamentous Actin and Tubular Recycling
624 Endosomes. *PLoS Genet* **12**, e1006093 (2016).
625 64. S. Chen *et al.*, SEC-10 and RAB-10 coordinate basolateral recycling of clathrin-independent cargo
626 through endosomal tubules in Caenorhabditis elegans. *Proc Natl Acad Sci U S A* **111**, 15432-
627 15437 (2014).

628

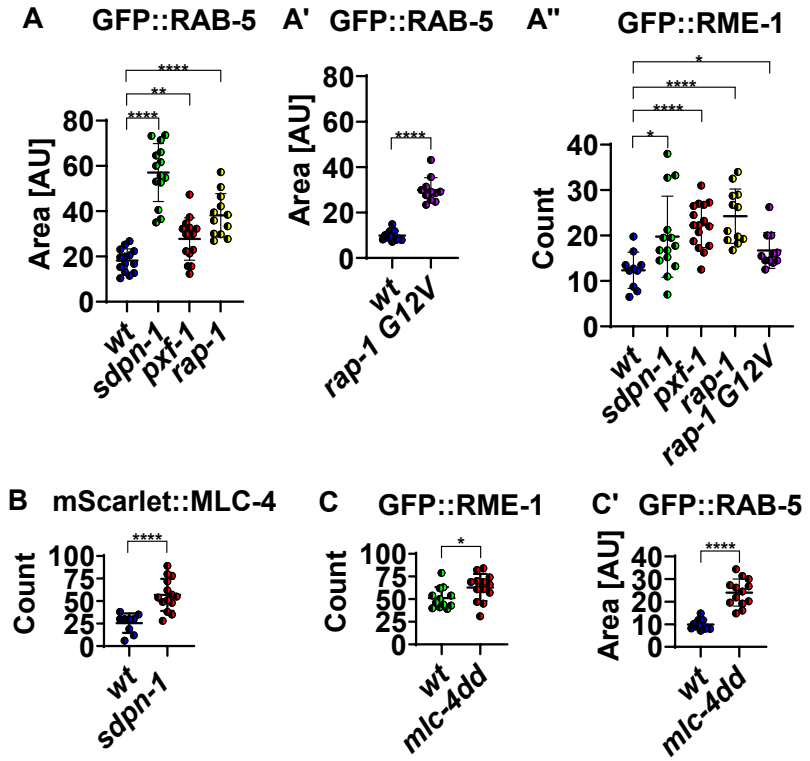

Figure S1. Additional quantification related to main figures 2, 5, and 6. (A-A'') ** Increased intracellular area labeled by GFP::RAB-5 and increased number of intracellular recycling compartments in interaction-defective mutants *sdpn-1(pw33)* and *pxf-1(pw34)*, as well as null *rap-1(tm861)* and activated *rap-1(re180)* (*rap-1 G12V*) mutants (related to Main Fig. 2A-C''''). **(B) Quantification of the number of intracellular mScarlet::MLC-4 regulatory myosin light chain puncta (related to Main Fig. 6C-C'). **(C-C')** Quantification of GFP::RME-1 labeled recycling compartments and intracellular area positive for early endosome marker GFP::RAB-5 (related to main Fig. 6E-H). Error bars represent SEM: *p< 0.05, **p< 0.01, **** p< 0.0001 (Two-tailed Welch's *t* test).

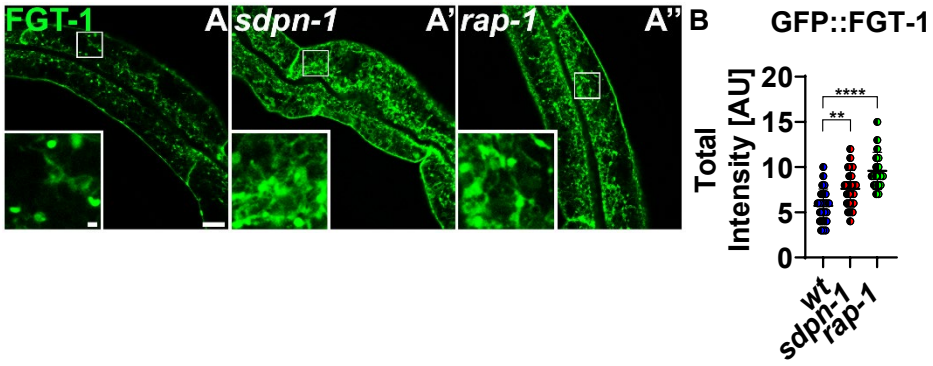

Figure S2. Intracellular accumulation of glucose transporter FGT-1 in *sdpn-1* and *rap-1 null* mutants. All micrograph images were obtained by confocal laser-scanning microscopy in intact living animals expressing intestine-specific GFP-tagged protein. **(A-A'')**. Representative images are shown for FGT-1::GFP in wild-type, *sdpn-1(ok1667),* and *rap-1(tm861)* mutants. Whole image scale bar = 10 µm. The panel at the bottom left of the image is the magnified section inside the white rectangle, scale bar = 1 µm. **(B)** Quantification of total intracellular fluorescence intensity. There is a significant increase in intracellular FGT-1::GFP accumulation in a *sdpn-1(0)* and *rap-1(0)* mutants compared to *wild-type*. Each data point represents one animal. Error bars represent SEM: ** $p<0.01$, **** $p< 0.0001$ (Two-tailed Welch's *t* test).

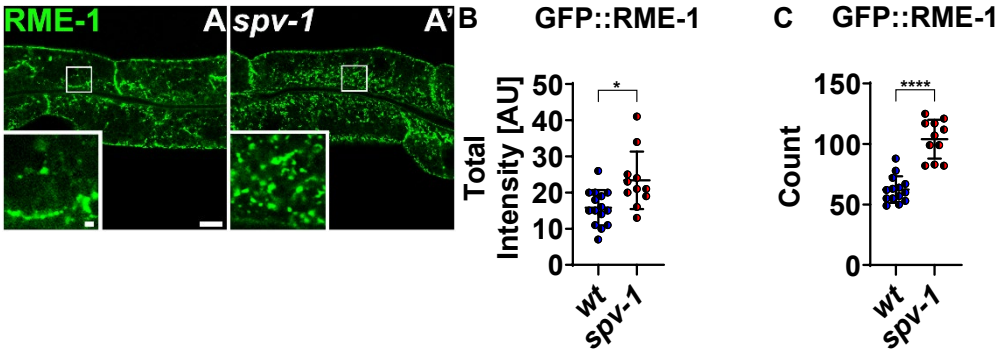

Figure S3. Loss of the SPV-1 Rho-GAP causes intracellular accumulation of RME-1-positive recycling endosomes. All micrograph images were obtained by confocal laser-scanning microscopy in intact living animals expressing intestine-specific GFP-tagged protein. **(A-A')** Representative images are shown for GFP::RME-1 labeled recycling endosome in wild-type and *spv-1(ok1498)* mutant animals. Whole image scale bar = 10 µm. The panel at the bottom left of the image is the magnified section inside the white rectangle, scale bar = 1 µm. **(B)** Quantification of total intracellular fluorescence intensity of recycling endosomes. **(C)** Quantification of the number of intracellular recycling endosomes. There is a significant increase in RME-1-positive recycling endosomes in *spv-1* mutants. Each data point represents one animal. Error bars represent SEM: * $p < 0.05$, **** $p < 0.0001$ (Two-tailed Welch's *t* test).

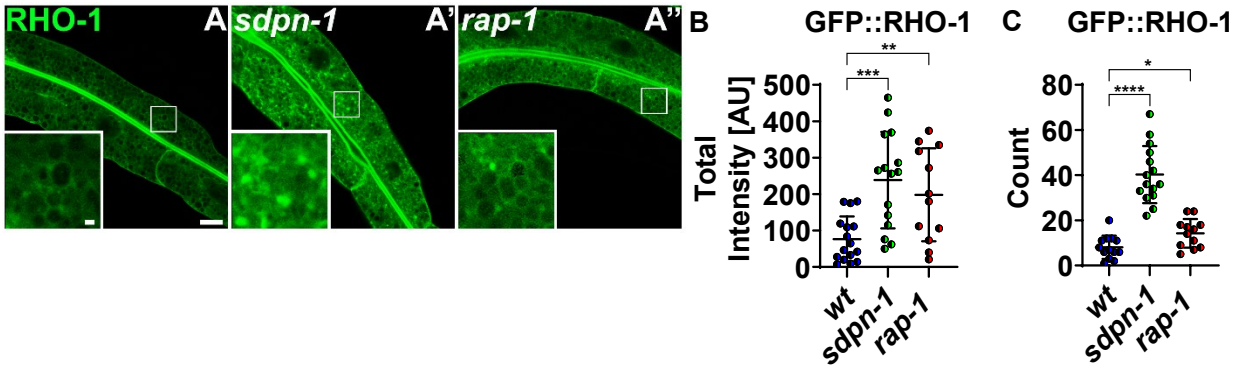

Figure S4. Intracellular RHO-1 signal increases in *sdpn-1* and *rap-1 null* mutants. All micrograph images were obtained via confocal laser-scanning microscopy in intact living animals expressing intestine-specific GFP-tagged protein. **(A-A'')** Whole image scale bar = 10 µm. The panel at the bottom left of the image is the magnified section inside the white rectangle, scale bar = 1 µm. **(B)** Quantification of total intracellular fluorescence intensity of RHO-1. **(C)** Quantification of the number of intracellular RHO-1 puncta. Intracellular puncta signal for GFP::RHO-1 increases significantly in *sdpn-1(ok1667)* and *rap-1(tm861)* mutants. Each data point represents one animal. Error bars represent SEM: * $p < 0.05$, ** $p < 0.01$, *** $p < 0.001$, **** $p < 0.0001$ (Two-tailed Welch's *t* test).

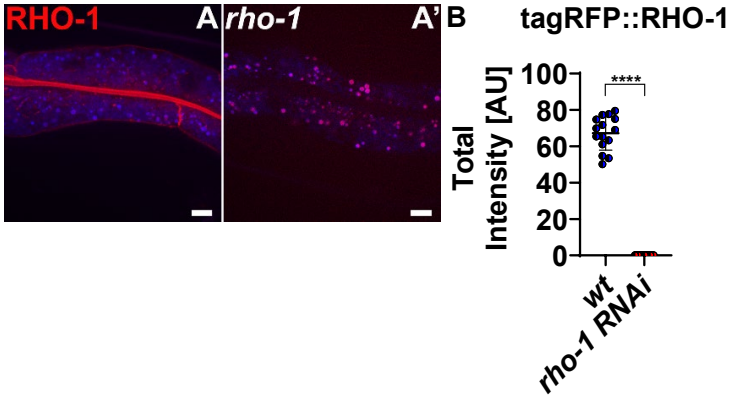

Figure S5. Intestinal RHO-1 was depleted by RHO-1 RNAi. All micrographs are from confocal image stacks acquired in intact living animals expressing intestine-specific RFP-tagged protein. **(A)** tagRFP::RHO-1 expression on a wild-type background. **(A')** tagRFP::RHO-1 is depleted by rho-1 RNAi. Scale bar = 10 µm. In each image, the blue channel denotes autofluorescent lysosome-like organelles, whereas the red channel denotes RFP. The red channel signal that does not overlap with the blue channel signal is considered bona fide RFP signal respectively. **(B)** Quantification of total fluorescence intensity. Each data point represents one animal. Error bars represent SEM: **** $p < 0.0001$ (Two-tailed Welch's *t* test).

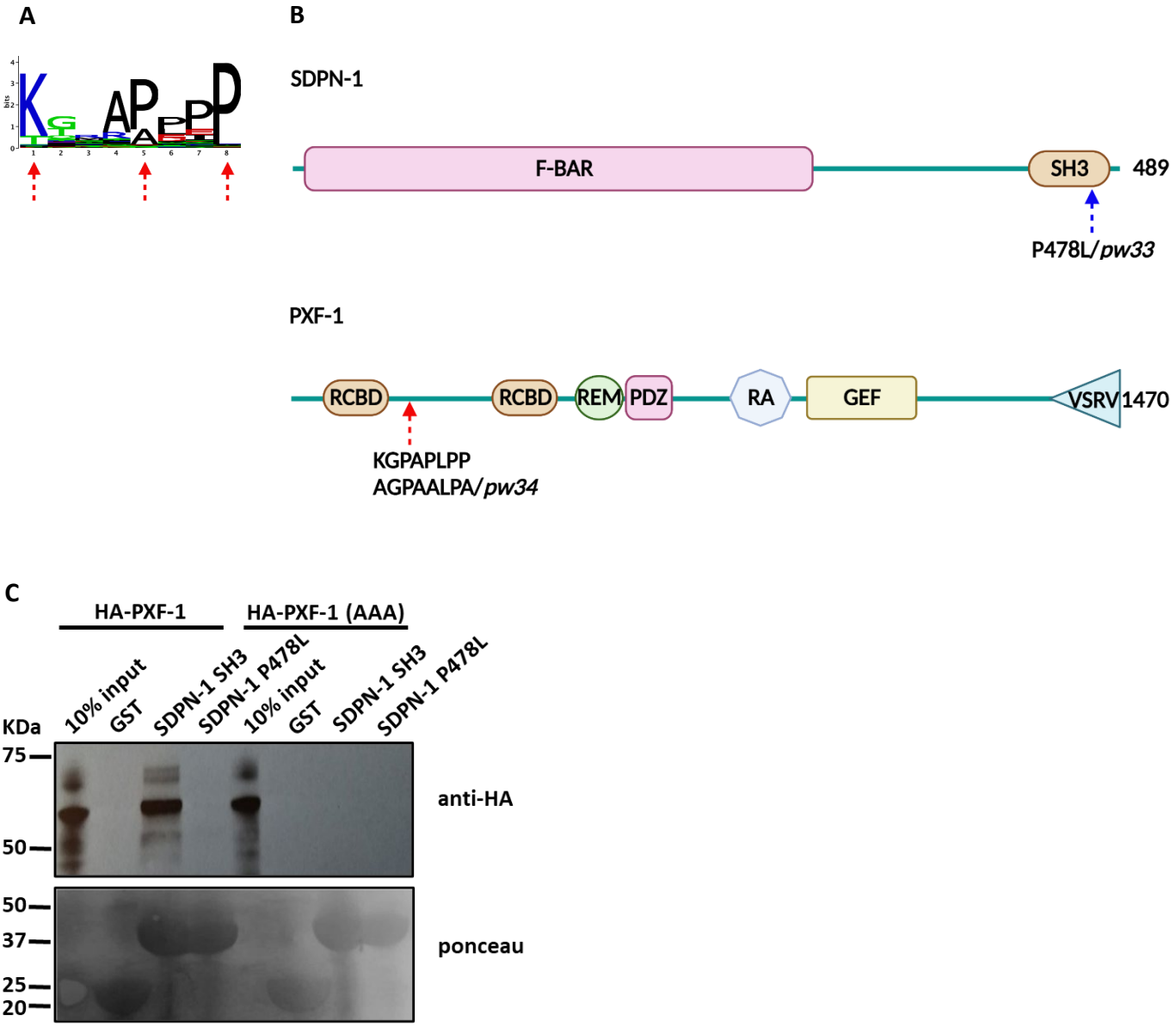

Figure 1. The SDPN-1 SH3 domain binds to PXF- 1. (A) SDPN-1 SH3 domain consensus target sequence; red arrows indicate conserved residues that were mutated to alanine (*pxf-1(pw34)*) to disrupt interaction with the SDPN-1 SH3 domain. **(B)** Schematic representation of SDPN-1 and PXF-1 domain structure from the N-terminal to the C-terminal; the blue arrow indicates the *sdpn-1(pw33)* mutation site and the red arrow indicates the *pxf-1(pw34)* mutation site. **(C)** Glutathione beads loaded with recombinant GST or the GST-SDPN-1 SH3 domain were incubated with *in vitro* translated HA-tagged PXF-1 *wild-type* or aa191-198 (**K**GPA**P**LP**P** to **A**GPA**A**LP**A**). Bound proteins were eluted and analyzed by Western blot probed with anti-HA antibody. The *wild-type* HA-tagged PXF-1 was bound by *wild-type* GST-SDPN-1-SH3, but not by mutant (P478L), or unfused GST. The (KGPAPLPP to AGPAALPA) mutant HA-tagged PXF-1 failed to bind GST alone or GST-SDPN-1-SH3 *wild-type* and mutant domains. Total GST and GST-SDPN-1-SH3 bait proteins were visualized by Ponceau Staining prior to antibody staining.

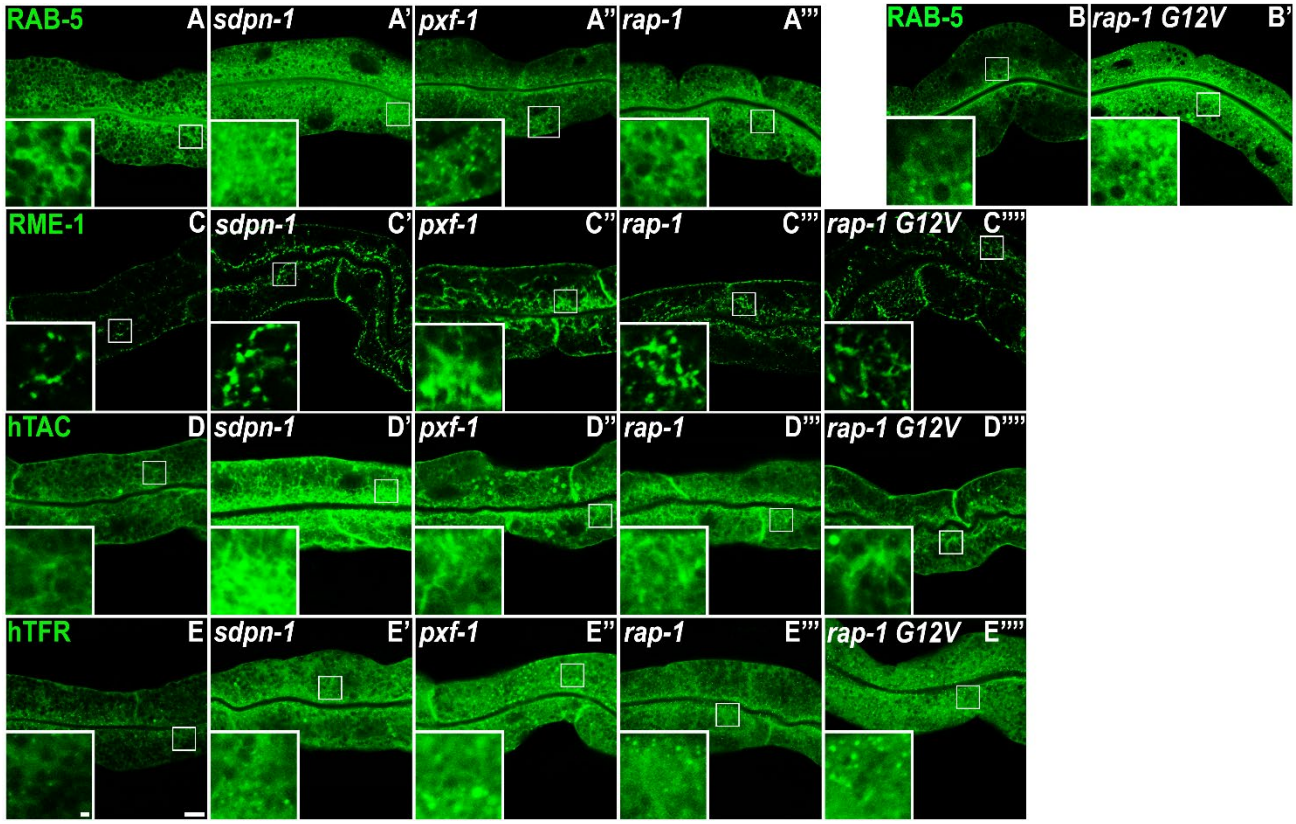
RAB-5 A
sdpn-1 A'
pxf-1 A''
rap-1 A'''
RAB-5 B
rap-1 G12V B'
RME-1 C
sdpn-1 C'
pxf-1 C''
rap-1 C'''
rap-1 G12V C''''
hTAC D
sdpn-1 D'
pxf-1 D''
rap-1 D'''
rap-1 G12V D''''
hTFR E
sdpn-1 E'
pxf-1 E''
rap-1 E'''
rap-1 G12V E''''

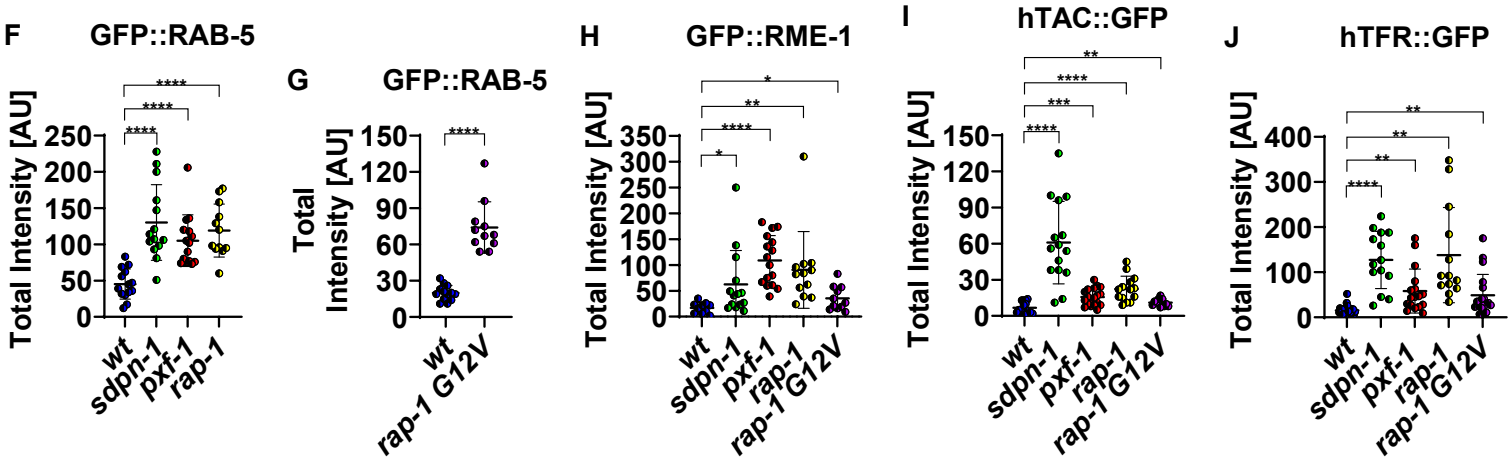
F GFP::RAB-5
Total Intensity [AU]
wt
sdpn-1
pxf-1
rap-1
G GFP::RAB-5
Total Intensity [AU]
wt
rap-1 G12V
H GFP::RME-1
Total Intensity [AU]
I hTAC::GFP
Total Intensity [AU]
J hTFR::GFP
Total Intensity [AU]

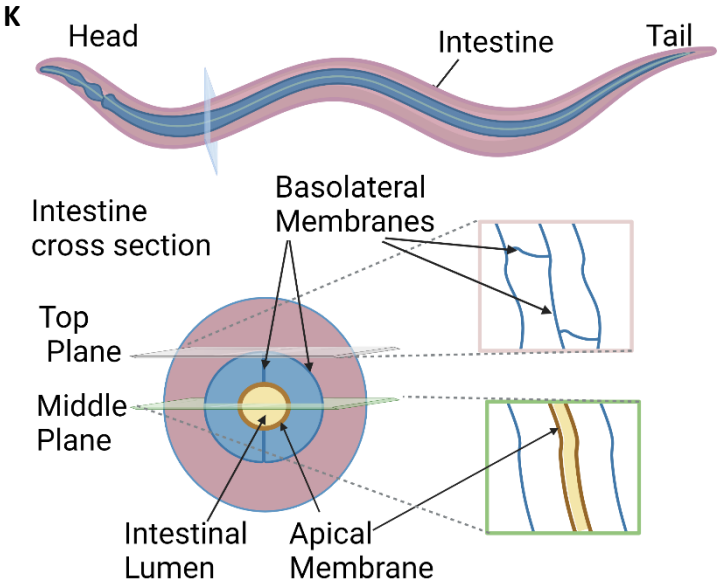
K
Head
Intestine
Tail
Intestine cross section
Basolateral Membranes
Top Plane
Middle Plane
Intestinal Lumen
Apical Membrane

Figure 2. SDPN-1 interaction with PXF-1, and RAP-1 is important for proper endocytic recycling. All images were obtained by confocal laser-scanning microscopy in intact living animals expressing intestine-specific GFP-tagged proteins. Representative confocal images of GFP::RAB-5 expressed in a *wild-type* **(A)**, *sdpn-1(pw33)* **(A')**, *pxf-1(pw34)* **(A'')**, and *rap-1(0)* **(A''')** background are shown. SDPN-1 and PXF-1 interacting-defective mutations, and loss of RAP-1, causes intracellular accumulation of compartments labeled by early endosome marker GFP::RAB-5 when compared with wild-type. In addition, GFP::RAB-5 expressed in a wild-type **(B)**, and *rap-1(re180)* GTP-locked mutant **(B')** background also showed an increase in the intracellular compartments labeled by early endosome marker GFP::RAB-5. Confocal images of GFP::RME-1 basolateral recycling endosome marker expressed in a *wild-type* **(C)**, *sdpn-1(pw33)* **(C')**, *pxf-1(pw34)* **(C'')**, *rap-1(0)* **(C''')**, and *rap-1(re180)* **(C'''')** background are shown. There is an increase of intracellular recycling compartments signal when SDPN-1 and PXF-1 interaction is lost, and when RAP-1 is missing or is GTP-locked. Micrographs showing representative confocal images of model GFP-tagged recycling cargo protein, the human interleukin-2 receptor (hTAC::GFP), expressed in a *wild-type* **(D)**, *sdpn-1(pw33)* **(D')**, *pxf-1(pw34)* **(D'')**, *rap-1(0)* **(D''')**, and *rap-1(re180)* **(D'''')** background. Micrographs showing representative confocal images of another model GFP-tagged recycling cargo protein, the human transferrin receptor (hTFR::GFP), expressed in a *wild-type* **(E)**, *sdpn-1(pw33)* **(E')**, *pxf-1(pw34)* **(E'')**, *rap-1(0)* **(E''')**, and *rap-1(re180)* **(E'''')** background. Losing the interaction between SDPN-1 and PXF-1, and when RAP-1 is missing or is GTP-locked, displays a significant increase in the intracellular accumulation of both recycling cargoes hTAC::GFP and hTFR::GFP. Main panel scale bars = 10 µm. Magnified inset panel scale bars = 1 µm. **(F)** Quantification of total fluorescence intensity for **(A-A''')**. **(G)** Quantification of total fluorescence intensity for **(B-B')**. **(H)** Quantification of total fluorescence intensity for **(C-C'''')**. **(I)** Quantification of total fluorescence intensity for **(D-D'''')**. **(J)** Quantification of total fluorescence intensity for **(E-E'''')**. **(K)** *C. elegans* intestinal diagram. Each data point represents one animal. Error bars represent SEM: *p< 0.05, **p< 0.01, *** p< 0.001, **** p< 0.0001 (Two-tailed Welch's *t* test).

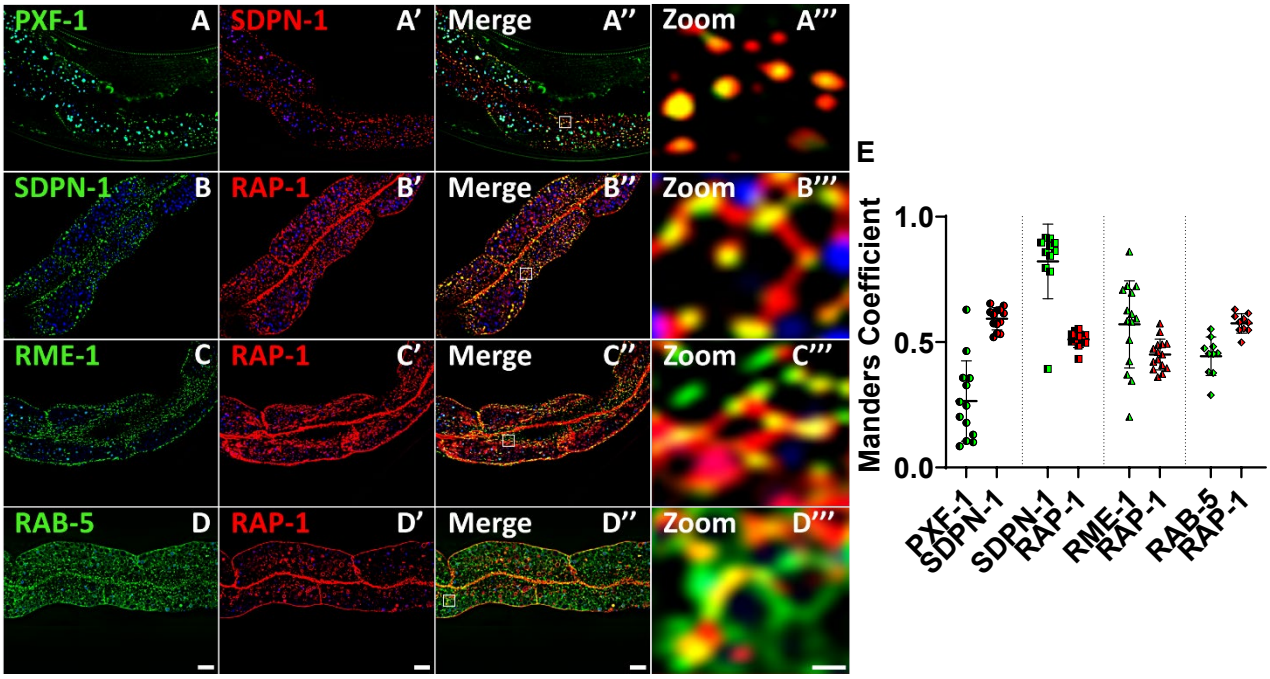

Figure 3. PXF-1 and RAP-1 are enriched on SDPN-1 positive endosomes. All micrographs are from three-dimensional (3D) confocal image stacks acquired in intact living animals expressing intestine-specific GFP and RFP-tagged proteins. **(A-A'')** GFP::PXF-1 is found on SDPN-1 positive compartments. **(A''')** Magnified image from the section designated by the white rectangle in panel A''. **(B-B'')** tagRFP::RAP-1 colocalizes with SDPN-1 positive endosomes. **(B''')** Magnified image from the section designated by the white rectangle in panel B''. **(C-C'')** tagRFP::RAP-1 is present in GFP::RME-1-labeled basolateral recycling endosomes. **(C''')** Magnified image from the section designated by the white rectangle in panel C''. **(D-D'')** There is colocalization between tagRFP::RAP-1 and GFP::RAB-5-labeled early endosomes. Scale bar = 10 µm. **(D''')** Magnified image from the section designated by the white rectangle in panel D''. Scale bar = 1 µm. In each image, the blue channel denotes autofluorescent lysosome-like organelles, whereas the green channel denotes GFP and the red channel denotes RFP. The green channel and red channel signal that do not overlap with the blue channel signal are considered *bona fide* GFP or RFP signals respectively. **(E)** Manders coefficient for colocalization of GFP::PXF-1 with tagRFP::SDPN-1, and tagRFP::RAP-1 with SDPN-1::GFP, GFP::RME-1 and GFP::RAB-5. Each data point represents one animal.

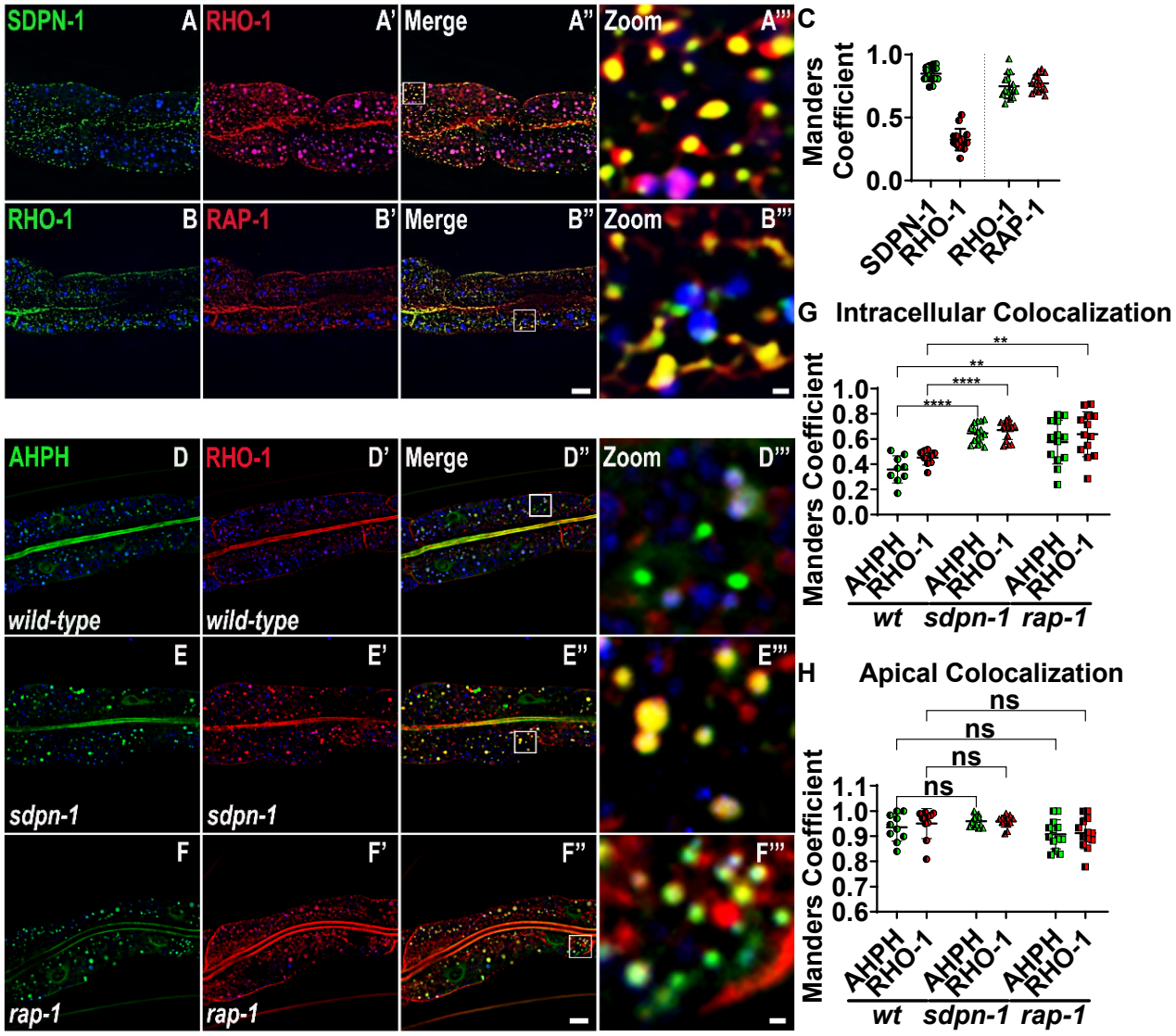

Figure 4. SDPN-1 and RAP-1 negatively regulate intracellular RHO-1 activation. All micrographs are from three-dimensional (3D) confocal image stacks acquired in intact living animals expressing intestine-specific GFP and RFP-tagged proteins. **(A-A'')** tagRFP::RHO-1 colocalizes extensively with SDPN-1 positive endosomes. **(A''')** Magnified image from the section designated by the white rectangle in panel **(A'')**. **(B-B'')** GFP::RHO-1 colocalizes with RAP-1 positive endosomes. Scale bar = 10 µm. **(B''')** Magnified image from the section designated by the white rectangle in panel **(B'')**. Scale bar = 1 µm. **(C)** Manders coefficient for colocalization of SDPN-1::GFP with tagRFP::RHO-1 and GFP::RHO-1 with tagRFP::RAP-1. **(D-F'')** Imaging of active RHO-1(GTP) via colocalization of RHO-1(GTP) biosensor AHPH with tagRFP::RHO-1 in wild-type, *sdpn-1(ok1667)*, and *rap-1(tm861)* backgrounds. Scale bar = 10 µm. **(D''-F'')** Magnified images from the section designated by the white rectangle in panel. Scale bar = 1 µm. **(D'''-F''')**. In each image, the blue channel denotes autofluorescent lysosome-like organelles, whereas the green channel denotes GFP and the red channel denotes RFP. The green channel and red channel signal that do not overlaps with the blue channel signal are considered bona fide GFP or RFP signals respectively. **(G)** Manders coefficient for intracellular colocalization of AHPH with RHO-1 in a *wild-type*, *sdpn-1 null* and *rap-1 null* background. Loss of SDPN-1 or RAP-1 results in an increased colocalization, indicating increased activation of RHO-1 in *sdpn-1* and *rap-1* mutants. **(H)** Manders coefficient for apical colocalization of AHPH with RHO-1 in a *wild-type*, *sdpn-1 null* and *rap-1 null* background. AHPH recruitment to apical RHO-1 is not increased in *sdpn-1* and *rap-1* mutants, supporting that the key site of action of SDPN-1 on RHO-1 is the endosomes and not the apical plasma membrane. Each data point represents one animal. Error bars represent SEM: ns (non-significant), **p< 0.01, **** p< 0.0001 (Two-tailed Welch's *t* test).

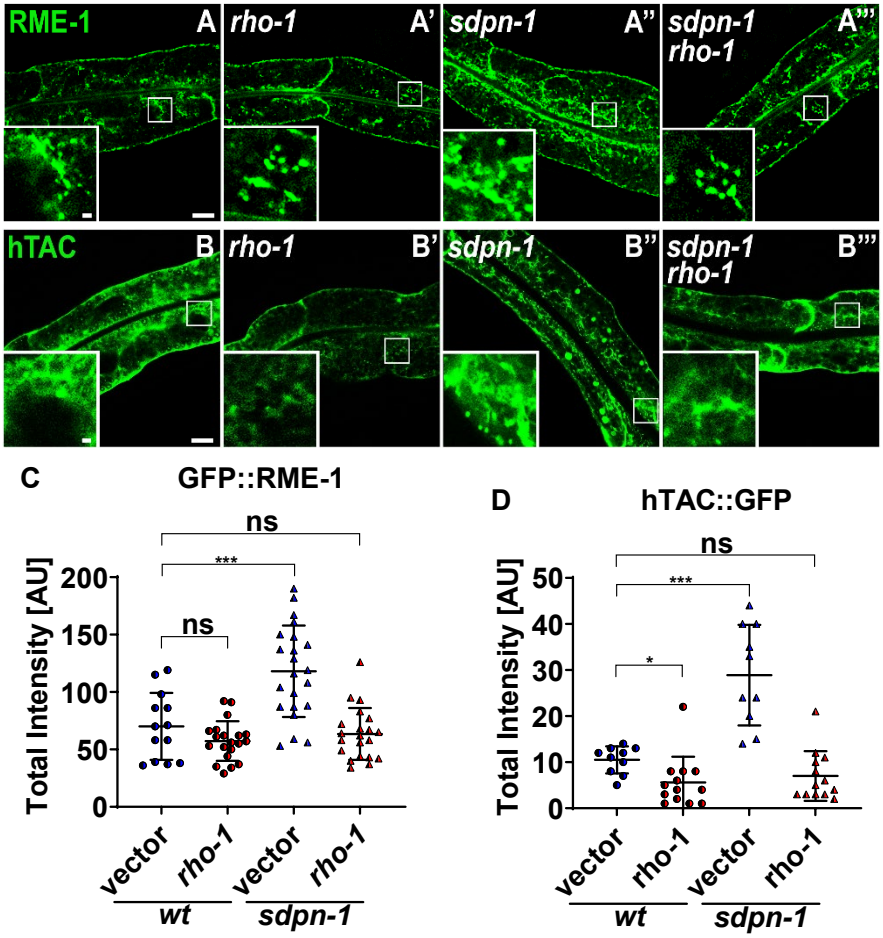

Figure 5. Depletion of RHO-1 suppresses *sdpn-1 null* mutant endocytic recycling phenotypes. All micrograph images were captured using confocal laser-scanning microscopy in intact living animals expressing intestine-specific GFP-tagged proteins. **(A-A')** GFP::RME-1 positive recycling endosomes visualized in otherwise *wild-type* animals after *empty-vector RNAi* or *rho-1* RNAi. **(A''-A''')** GFP::RME-1 positive recycling endosomes visualized in *sdpn-1(ok1667)* mutant animals after *empty-vector RNAi* or *rho-1* RNAi. **(B-B')** Recycling cargo hTAC::GFP was visualized in otherwise *wild-type* animals after *empty-vector RNAi* or *rho-1* RNAi. **(B''-B''')** Recycling cargo hTAC::GFP was visualized in *sdpn-1(ok1667)* mutant animals after *empty-vector RNAi* or *rho-1* RNAi. Whole image scale bar = 10 µm. The panel at the bottom left of the image is the magnified section inside the white rectangle, scale bar = 1 µm. **(C)** Quantification of intracellular total fluorescence intensity for **(A-A''')**. *sdpn-1(ok1667)* mutant animals display an intracellular increase of GFP::RME-1-positive recycling endosomes. This phenotype is suppressed by *rho-1 RNAi* knockdown. **(D)** Quantification of intracellular total fluorescence intensity for **(B-B''')**. *sdpn-1(ok1667)* mutant animals accumulate abnormally high levels of intracellular recycling cargo hTAC::GFP. This phenotype is suppressed by *rho-1 RNAi* knockdown. Each data point represents one animal. Error bars represent SEM: ns (non-significant), *p< 0.05, ***p< 0.001 (Two-tailed Welch's *t* test).

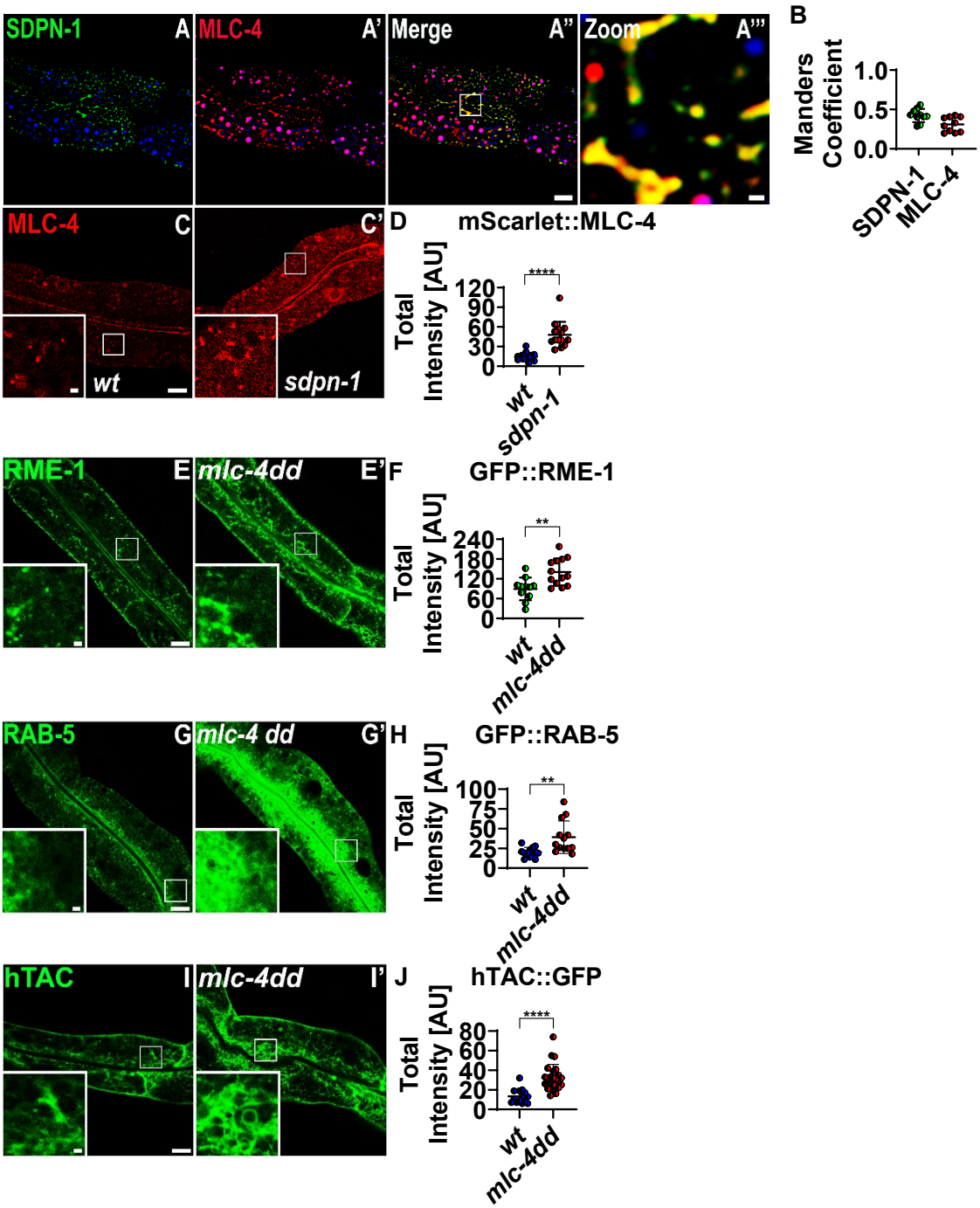

Figure 6. Non-muscle myosin II associates with SDPN-1-positive endosomes and modulates their function. (A-A'') Confocal images comparing the subcellular localization of SDPN-1::GFP-positive endosomes and myosin light chain mScarlet::MLC-4 in the intestine of intact living animals. Most of SDPN-1 positive compartments are enriched in myosin light chain (MLC-4). Scale bar = 10 µm. **(A''')** Magnified image from the section designated by the white rectangle in panel **(A'')**. Scale bar = 1 µm. In each image, the blue channel denotes autofluorescent lysosome-like organelles, whereas the green channel denotes GFP and the red channel denotes mScarlet. The green channel and red channel signal that does not overlaps with the blue channel signal are considered *bona fide* GFP or mScarlet signals respectively. **(B)** Manders coefficient for colocalization of SDPN-1::GFP with mScarlet::MLC-4 indicates strong enrichment for MLC-4 on endosomes. **(C-C')** The signal of intracellular myosin light chain (mScarlet::MLC-4) positive compartments increases in a *sdpn-1(ok1667)* mutant background. **(D)** Quantification intracellular total fluorescence intensity for **(C-C')**. **(E-H)** Animals expressing a constitutively active myosin light chain phospho-mimetic protein MLC-4DD in the intestine display increased intracellular accumulation of early and recycling endosomes. **(I-J)** Animals expressing a constitutively active myosin light chain phospho-mimetic protein MLC-4DD in the intestine display an increase in intracellular recycling cargo hTAC::GFP. Each data point represents one animal. Error bars represent SEM: **p< 0.01, **** p< 0.0001 (Two-tailed Welch's *t* test).

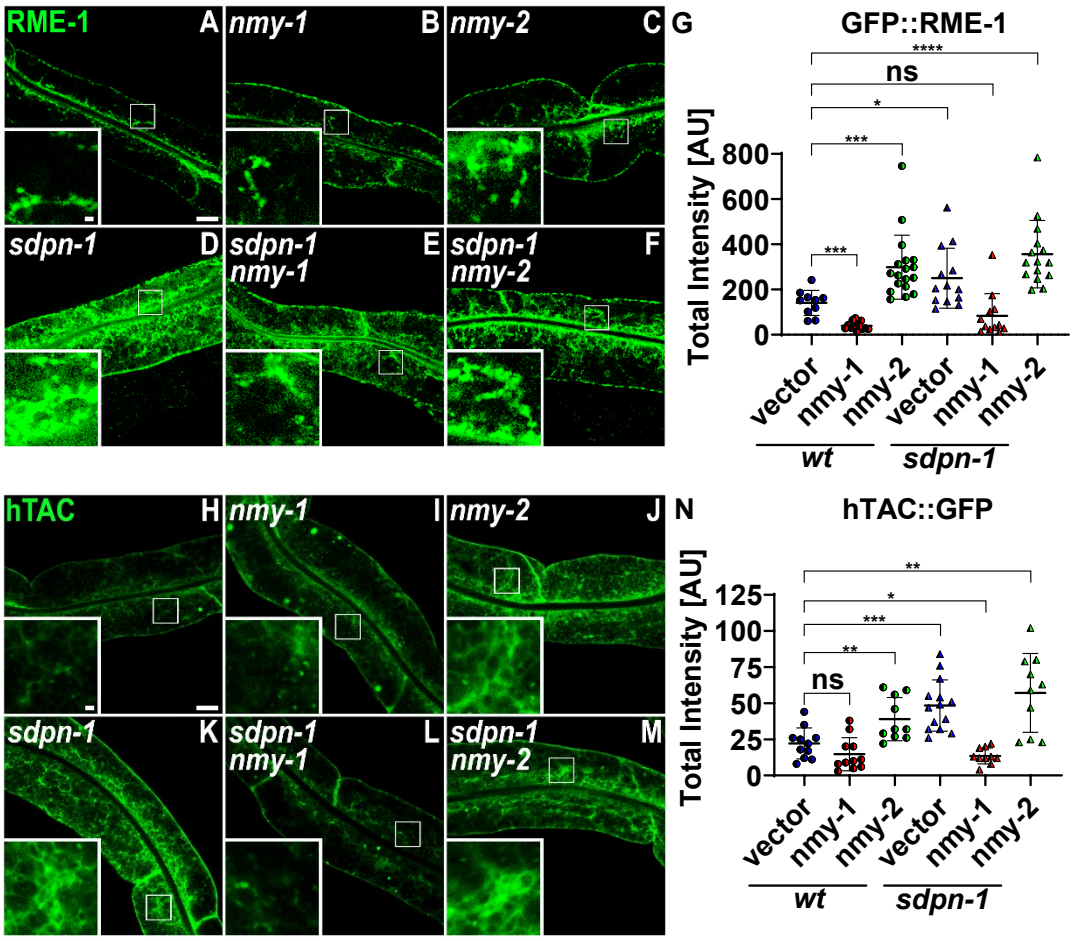

Figure 7. Opposing requirements for non-muscle myosin heavy chains on endocytic recycling. All micrograph images were captured using confocal laser-scanning microscopy in intact living animals expressing intestine-specific GFP-tagged proteins. **(A-C)** GFP::RME-1 positive recycling endosomes visualized in otherwise *wild-type* animals after *empty-vector* RNAi, *mny-1* RNAi or *nmy-2* RNAi. **(D-F)** GFP::RME-1 positive recycling endosomes visualized in *sdpn-1(ok1667)* mutant animals after *empty-vector* RNAi, *nmy-1* RNAi or *nmy-2* RNAi. Whole image scale bar = 10 µm. The panel at the bottom left of the image is the magnified section inside the white rectangle, scale bar = 1 µm. **(G)** Quantification of intracellular total fluorescence intensity for **(A-F)**. *sdpn-1(ok1667)* mutant animals display an increase of intracellular GFP::RME-1-positive recycling endosomes. This phenotype is suppressed by *nmy-1 RNAi* knockdown, but phenocopied by *nmy-2 RNAi* knockdown. **(H-J)** Recycling cargo hTAC::GFP visualized in otherwise *wild-type* animals after *empty-vector* RNAi, *mny-1* RNAi or *nmy-2* RNAi. **(K-M)** Recycling cargo hTAC::GFP visualized in *sdpn-1(ok1667)* mutant animals after *empty-vector* RNAi, *nmy-1* RNAi or *nmy-2* RNAi. Whole image scale bar = 10 µm. The panel at the bottom left of the image is the magnified section inside the white rectangle, scale bar = 1 µm. **(N)** Quantification of intracellular total fluorescence intensity for **(H-M)**. *sdpn-1(ok1667)* mutant animals accumulate abnormally high levels of intracellular recycling cargo hTAC::GFP. This phenotype is suppressed by *nmy-1 RNAi* knockdown, but phenocopied by *nmy-2 RNAi* knockdown. Each data point represents one animal. Error bars represent SEM: ns (non-significant), *p< 0.05, **p< 0.01, ***p< 0.001, ****p< 0.0001 (Two-tailed Welch's *t* test).

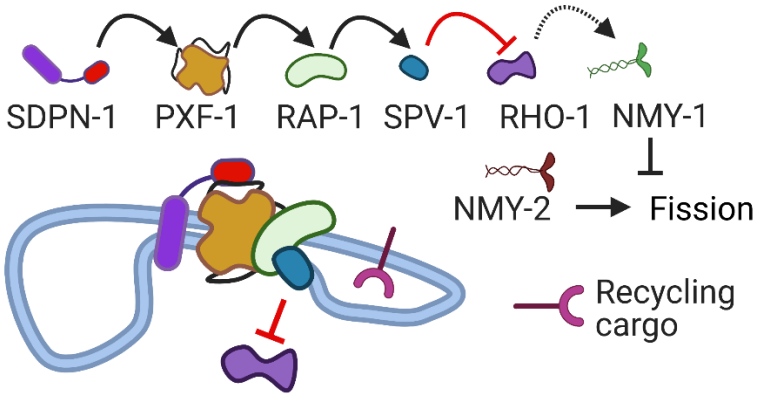

Figure 8. Model: SDPN-1 differentially regulates Non-Muscle Myosins via RAP-1 to RHO-1 signaling to regulate endocytic recycling. Recycling tubules pulled from sorting endosomes require non-muscle myosin NMY-2, likely for tubule fission. The F-BAR protein SDPN-1/Syndapin and its binding partner PXF-1 activate RAP-1/Rap to restrain the level of RHO-1/RhoA and non-muscle myosin NMY-1 activity on the endosome. Such negative regulation is required for successful recycling.